Journal of Theoretical Biology 604 (2025) 112050

Contents lists available at ScienceDirect

Journal of Theoretical Biology

journal homepage: www.elsevier.com/locate/yjtbi

Tradeoffs in the energetic value of neuromodulation in a closed-loop neuromechanical system

Zhuojun Yu [a,b,*], Yangyang Wang [c], Peter J. Thomas [a], Hillel J. Chiel [d]

[a] Department of Mathematics, Applied Mathematics, and Statistics, Case Western Reserve University, Cleveland, OH 44106, USA
[b] Department of Psychology & Neuroscience Institute, Carnegie Mellon University, Pittsburgh, PA 15213, USA
[c] Department of Mathematics, Brandeis University, Waltham, MA 02453, USA
[d] Department of Biology, Department of Neuroscience, and Department of Biomedical Engineering, Case Western Reserve University, Cleveland, OH 44106, USA

ARTICLE INFO

Keywords:
Neuromodulation
Energetics
Muscle
Central pattern generator
Neuromechanics
Closed-loop control

ABSTRACT

Rhythmic motor behaviors controlled by neuromechanical systems, consisting of central neural circuitry, biomechanics, and sensory feedback, show efficiency in energy expenditure. The biomechanical elements (e.g., muscles) are modulated by peripheral neuromodulation which may improve their strength and speed properties. However, there are relatively few studies on neuromodulatory control of muscle function and metabolic mechanical efficiency in neuromechanical systems. To investigate the role of neuromodulation on the system's mechanical efficiency, we consider a neuromuscular model of motor patterns for feeding in the marine mollusk *Aplysia californica*. By incorporating muscle energetics and neuromodulatory effects into the model, we demonstrate tradeoffs in the energy efficiency of *Aplysia*'s rhythmic swallowing behavior as a function of the level of neuromodulation. A robust efficiency optimum arises from an intermediate level of neuromodulation, and excessive neuromodulation may be inefficient and disadvantageous to an animal's metabolism. This optimum emerges from physiological constraints imposed upon serotonergic modulation trajectories on the energy efficiency landscape. Our results may lead to experimentally testable hypotheses of the role of neuromodulation in rhythmic motor control.

1. Introduction

Many physiological systems underlying fundamental behaviors, such as breathing, feeding, flying, and walking, must generate rhythmic motor patterns that are *energetically efficient* so as to adapt to continuously changing internal or external conditions. These systems are driven by brain-body interactions through a *closed-loop* architecture consisting of central neural circuitry, biomechanics, and sensory feedback (Chiel and Beer, 1997; Kuo, 2002; Spardy et al., 2011; Diekman et al., 2017; Yu and Thomas, 2021). Such a control architecture endows the systems with central and peripheral plasticity, which are partially mediated by *endogenous chemical neuromodulation* — the ability of certain substances such as serotonin and peptides to modulate the responses of other neurons to changing inputs.

Energy is critical to the ability of animals to generate behaviors and plays a central role in allowing muscles to perform a wide range of tasks. A majority of activities, including swimming (Rodríguez and Mader, 2011), jumping (James et al., 2007), and running (Hultman and Greenhaff, 1991), require the rapid production of mechanical energy by muscle contraction. In these activities, the power output and energy efficiency of muscles, which vary widely under different contractile conditions, are maximized for behavioral performance.

Muscle contractile properties are subject to neuromodulation, which acts to regulate its strength and speed (Weiss et al., 1978; Kupfermann, 1979; Hooper et al., 1999; Hurwitz et al., 2000). For instance, Deodhar and Kupfermann (2000) investigated the effects of neuromodulation on buccal muscles that execute feeding movements, and they showed that the enhancement of the rate of muscle relaxation and the force of muscle contraction by neuromodulation could lead to a recovery of the fitness (defined to be the difference between energy gained from food and energy expended by muscle activity) that is lost when the feeding pattern generator is slowed down by an external influence. In addition, Liessem et al. (2021) showed that stick insect leg muscles are innervated by a neuron containing one neuromodulator (myoinhibitory peptide), which specifically increases the muscle's ability to contract and relax rapidly, enhancing fast movements. All these previous studies suggest that neuromodulation plays an important role in improving both muscle function and behavioral efficiency.

* Correspondence to: Department of Psychology & Neuroscience Institute, Carnegie Mellon University, Pittsburgh, PA 15213, USA.
E-mail address: zhuojuny@andrew.cmu.edu (Z. Yu).

https://doi.org/10.1016/j.jtbi.2025.112050
Received 8 June 2024; Received in revised form 17 December 2024; Accepted 21 January 2025
Available online 30 January 2025

Consider energetics related to neuromodulatory processes in tuning the overall muscle performance during feeding. On the one hand, modulators act on the muscle to affect its dynamic properties such that more food and energy are gained by the stronger and faster muscle. On the other hand, previous studies have revealed that the modulators also play a significant role in altering the basal metabolism of muscle, as seen from increasing oxygen consumption, heat liberation, as well as glucose uptake and utilization (Mansour, 1959; Moore et al., 1961; Baguet and Gillis, 1967; Twarog, 1968). Therefore, the up-regulation of muscle by neuromodulators is also energetically costly to the system. However, if spending more energy on neuromodulation can lead to more efficient muscle performance and successful ingestion of even more energy, then it might be more advantageous to have higher metabolic muscle costs than the metabolic costs at rest. To our knowledge, no one has developed a mathematical model accounting for the energetic tradeoffs associated with neuromodulation.

The goal of this work is to establish the relationship between energetic efficiency and neuromodulation in a closed-loop neuromuscular system. To mathematically model neuromodulatory effects on behavioral fitness, we need a system in which key elements for closed-loop control are included and many of the details have been experimentally measured. The marine mollusk *Aplysia* has been used widely as a model system to understand the brain-body control mechanisms for producing robust and adaptive behavior in a dynamic environment because of the relatively small number of neurons in its nervous system (Kandel, 1979). Feeding behavior of the animal also shares certain fundamental features with that of many vertebrates (Kupfermann, 1974). In addition, there is already a substantial corpus of neurophysiological and behavioral studies on feeding in *Aplysia*, including the energetics of feeding in *Aplysia* (Carefoot, 1967, 1970) as well as the serotonergic and peptidergic modulation of *Aplysia*'s buccal muscles (Cropper et al., 1994; Hurwitz et al., 2000).

Shaw et al. (2015) and Lyttle et al. (2017) developed a closed-loop neuromechanical model of motor patterns for the rhythmic feeding behavior of *Aplysia californica*, which allows one to quantitatively study rhythm generation and modulation. Specifically,

- Shaw et al. (2015) showed that a central pattern generator model based on a stable heteroclinic channel type of dynamical architecture provided a better match to the distribution of durations of different subcomponents of rhythmic feeding movements than a more standard limit cycle based model.
- Lyttle et al. (2017) demonstrated that the Shaw et al.'s model possessed a parameter range with multistability and that access to a repertoire of different movements allowed for more efficient feeding in a mixed ongoing biting/swallowing task setting.
- Wang et al. (2022) showed how newly developed mathematical tools – variational analysis of shape and timing for nonsmooth limit cycle systems (Wang et al., 2021) – could shed light onto the mechanism by which sensory feedback and nonlinear biomechanical elements together produced robust feeding movements that maintained efficiency (rate of seaweed intake) despite increases in mechanical loads opposing ingestion.
- In Yu et al. (2023), the tools developed in Wang et al. (2021) that were applied to the model (in Wang et al. 2022 as just described) were further applied to a simplified (piecewise linear) variant of the central pattern generator circuit from the *Aplysia* neuromechanical model in order to compare regulation by descending control mechanisms in that system versus in alternative rhythm generation systems (threshold linear network systems and coupled relaxation oscillator systems).

The above studies using the *Aplysia* feeding neuromechanical model provide insights into the function of other motor systems as well. However, this prior work has not considered energetics, nor neuromodulatory effects. In the present paper we augment the previously established model by incorporating muscle energetics and neuromodulation, and we seek to understand the role of neuromodulatory control in the biomechanical power output and efficiency.

An important result of the work presented here is that we observe neuromodulatory tradeoffs in the energy efficiency of the rhythmic behavior. Two major findings are (1) the existence of a single efficiency optimum for serotonin in the model, and (2) the emergence of this optimum from physiological constraints imposed upon serotonergic modulation trajectories on the energy efficiency landscape. Thus, our paper is likely to provide insights into the neuromodulatory control of metabolism in other motor systems, which can lead to testable predictions to study rhythm modulation and motor control in the context of behavioral fitness.

We organize the rest of our paper as follows. We describe the neuromechanical model, incorporating muscle energetics and neuromodulation, in Section 2. Section 3 presents the main analysis and results on the neuromodulatory tradeoffs. Finally, in Section 4 we discuss limitations, connections to previous literature, and possible implications of our results for experiments and future work.

2. Model description

This section presents a brief description of the specific neuromechanical model we study (Section 2.1), followed by modeling work on muscle energetics (Section 2.2) and neuromodulation (Section 2.3) to provide the basis for our analysis. More details and modeling background are given in Appendices A, B, and C.

2.1. Neuromechanical model

The neuromechanical model we consider for *Aplysia*'s ingestive behavior is a nominal, triphasic, rhythmic motor pattern generator, adapted from Shaw et al. (2015) and Lyttle et al. (2017). The model divides the swallowing into three phases — protraction-open, protraction-closed, and retraction, representing the mechanics of a feeding grasper, see Fig. 1A. To ingest food, the grasper is moved forward (protraction-open), closes on the food (protraction-closed), and then is moved backward into the buccal cavity (retraction). A buccal muscle, referred to as I2, protracts the grasper, and another buccal muscle, called I3, retracts the grasper to pull the grasped food into the buccal cavity to complete swallowing.

As shown in Fig. 1B, each of the three phases is controlled by the activation of one of three neural pools, represented by firing rates a_0, a_1, and a_2, respectively. The three neural components have inhibitory synaptic connections that mediate the rhythmic motor pattern generation. In addition, each pool receives a source of endogenous neural excitation. The I2 muscle activation (u_0) is driven by both protraction-open (a_0) and protraction-closed (a_1) neural pools, whereas the I3 muscle activation (u_1) is driven by the single retraction neural pool (a_2). The tension in each muscle is assumed to follow a simplified Hill-type kinetic model, determined by its activation and kinematics (length). The sum of a_1 and a_2 exceeding a threshold induces the grasper to close; otherwise, it is open. The movement of the grasper, whose position is denoted as x_r, is controlled by the net force exerted on it, and an external load from food is present only when the grasper is closed on food.

Finally, to form a closed-loop system, input from proprioceptive feedback is integrated into each neural pool as a function of the grasper position. Proprioception provides essential information about the state of the body, allowing the nervous system to adjust its output accordingly, facilitating more adaptive and flexible movement in response to a changing world. In this way, the combined dynamics of the neural system, biomechanics, and periphery make it possible to generate robust feeding rhythms. The specific equations for the entire model and values of model parameters are given in Appendix A. For more modeling details, see Shaw et al. (2015) and Lyttle et al. (2017).

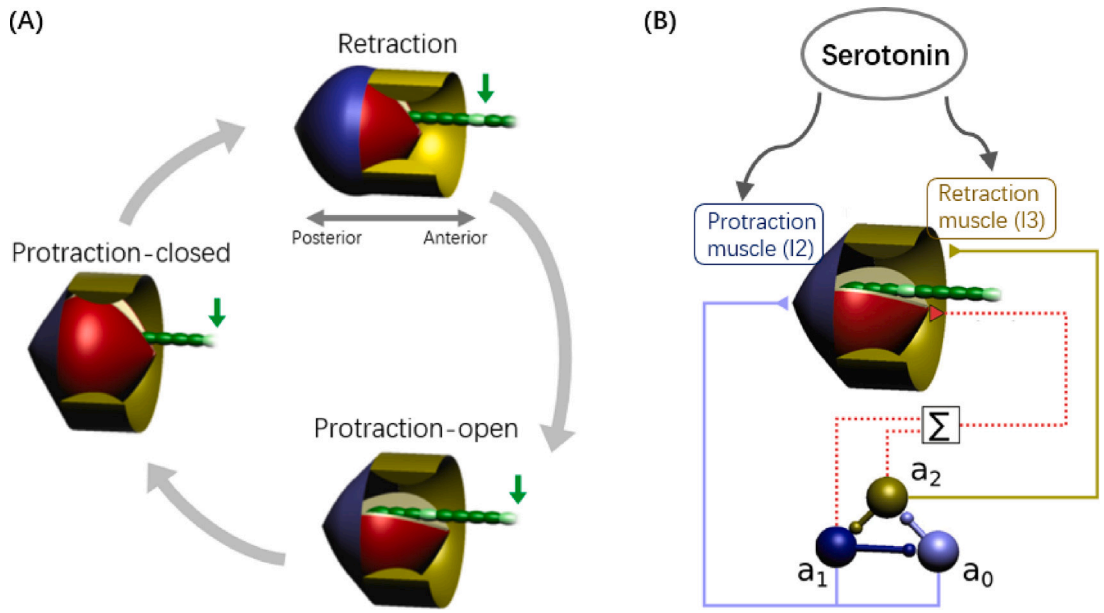

Fig. 1. (A) Schematic of *Aplysia* swallowing, consisting of three phases. During the protraction-open phase (lower right), the grasper (red), which stays open to grasp food, is protracted (moves forward) by the I2 buccal muscle (blue). Then the grasper begins closing on the food and is protracted a small distance while closed, referred to as protraction-closed phase (left middle). In the last phase, retraction phase (upper right), the I3 buccal muscle (yellow) retracts the grasper backwards to pull the food into the buccal cavity, completing the swallowing cycle. The seaweed is indicated by the green strand, with the green arrows showing how the seaweed moves within a cycle. **(B)** Three neural pools, with firing rates denoted by a_0, a_1, a_2, control the three phases. The protraction muscle I2 is driven by the neural inputs from a_0 and a_1 (blue solid line and triangle), and the retraction muscle I3 receives neural inputs from a_2 (yellow solid line and triangle). The grasper is closed when the sum of a_1 and a_2 exceeds a threshold and is open otherwise, as represented by the red dashed line and summation symbol. Serotonin, as a neuromodulatory substance, acts in part on the two buccal muscles (gray arrows).
Source: Figure redrawn from Shaw et al. (2015).

As a reference, Fig. 2 shows the trajectory of the (default) system in the absence of neuromodulation with parameters values listed in Table 1, from the start of the grasper-closed phase. The dynamics of the system exhibits a stable periodic limit-cycle behavior with period $T = 6.44$ s. The firing rate of each neural component a_i is nonnegative, and may drop to zero if the neural pool receives more inhibition than excitation. In this case, the neural pool remains insensitive to further inhibition, and its firing rate will remain at zero until its excitatory input exceeds its inhibitory input. The grasper position x_r provides a quantitative length measure of seaweed ingested per swallowing cycle, defined to be the net change of x_r during the grasper-closed phase (gray shaded regions). In the following, we add to this neuromechanical model muscle energetics and neuromodulation to investigate the trade-offs associated with neuromodulation: enhanced feeding versus increased metabolic costs.

2.2. Smooth muscle energetics

Mechanical *efficiency* of muscle activity quantifies the fraction of energy utilized by a muscle that functions as external work, defined by

$$\text{Efficiency} = \frac{\text{Work}}{\text{Work} + \text{Heat}}.$$

The work is the intergral of the muscle force over the working length and heat is the heat produced by the muscle. In this section, we apply a modified Hill-type muscle model (Hill, 1938; Lichtwark and Wilson, 2005) to *Aplysia*'s buccal muscles, I2 and I3, to predict their energetics. The model enables us to evaluate the energetic costs due to the heat production in each swallow cycle of *Aplysia*. Then, by using *work loop* analysis, we determine the muscles' work output and the efficiency of muscle contractions.

Heat output Muscle energy usage differs throughout three different types of contraction activity — isometric contraction, shortening contraction, and lengthening contraction,[1] each of which has different energetic characteristics.[2] The overall heat production from a muscle, denoted by H, consists of four components — the 'stable' heat H_M, the 'labile' heat H_L, the 'shortening' heat H_S, and the 'thermoelastic' heat H_T (Lichtwark and Wilson, 2005):

$$H = H_M + H_L + H_S + H_T.$$

The stable heat describes the minimum heat required to produce an isometric force at any given activation state, which is determined by the crossbridge activation level (Act). Unlike H_M, the stable heat, the heat production rate during a contraction is not constant, usually declining exponentially from a high initial rate to a lower value (Aubert and Hill, 1956). The labile heat accounts for the rapidly decaying component. The shortening heat is the extra heat output associated with muscle's shortening at any given activation level, which is dependent on Act and the velocity of the contractile element (V_{CE}). The thermoelastic heat results from the heat absorption by the muscle, associated with the muscle's instantaneous force (P). During shortening contractions, the rate of change of the four heat components is modeled as four distinct functions:

$$\begin{aligned}\frac{dH}{dt} &= \frac{dH_M}{dt} + \frac{dH_L}{dt} + \frac{dH_S}{dt} + \frac{dH_T}{dt} \\ &= f_1(\text{Act}) + f_2^S(\text{Act}, t) + f_3^S(\text{Act}, V_{\text{CE}}) + f_4^S(P),\end{aligned}$$

where the superscript in f_i^S denotes shortening.

[1] Following standard terminology in the muscle physiology literature, a "lengthening contraction" denotes the muscle lengthening due to externally applied forces that exceed the contractile tension actively generated by the muscle.

[2] In mammalian smooth muscles, for example rabbit taenia coli, the average rate of energy expenditure during shortening with isovelocity conditions (initiated after isometric tension) is about 2.5 times the rate during force maintenance under isometric conditions (Butler et al., 1983). In contrast, the muscle's stretch decreases the average rate of energy usage compared to that under isometric conditions (Butler et al., 1983).

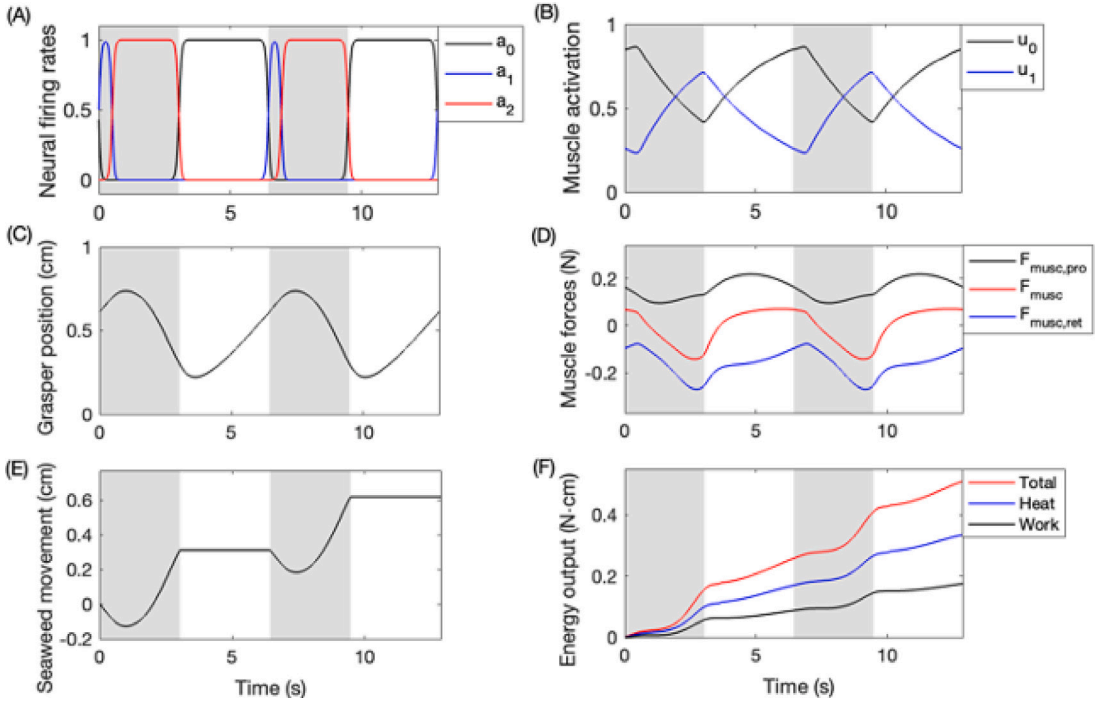

Fig. 2. Time courses for the default system (in the absence of neuromodulation) of **(A)** firing rates of neural pools (a_0, a_1, a_2), **(B)** muscle activation (u_0, u_1), **(C)** grasper position (x_r), **(D)** protractor muscle force $(F_{\text{musc,pro}})$, retractor muscle force $(F_{\text{musc,ret}})$, and total muscle force $(F_{\text{musc}} = F_{\text{musc,pro}} + F_{\text{musc,ret}})$, **(E)** seaweed movement, and **(F)** energy output (Total = Work + Heat), plotted over two periods with $T = 6.44$ s. The gray shaded regions denote the phase when the grasper is closed (protraction-closed and retraction), with duration $T_{\text{closed}} = 3.03$ s; the white regions indicate the phase when the grasper is open (protraction-open), with duration $T_{\text{open}} = 3.41$ s. The seaweed moves together with the grasper during the grasper-closed phase in a rate $-dx_r/dt$, while it does not move when the grasper is open (compare panels (C) and (E)).

The active lengthening contraction, in contrast, reduces the heat output compared with the isometric contraction. The minimum heat rate is at least 30% of the stable heat rate used to activate the muscle, and the rate of heat production decays exponentially as the lengthening velocity increases. One further factor, the muscle's stretch and absorption of work, also becomes heat within a short period of time. Hence, the heat production rate during lengthening contractions can be approximated by

$$\begin{aligned}\frac{dH}{dt} &= 0.3\frac{dH_M}{dt} + \frac{dH_L}{dt} + \frac{dH_S}{dt} \\ &= 0.3 f_1(\text{Act}) + f_2^L(\text{Act}, P) + f_3^L(V_{\text{CE}}, P),\end{aligned}$$

where the superscript in f_i^L refers to lengthening. For the equations of the energetic model, see Appendix B. Fig. 2F plots the time course of the heat liberated (blue curve) in the default system.

Work output Muscles undergoing shortening contractions generate mechanical work; in contrast, work is done on muscles during lengthening contractions, which means energy is stored by the muscles and will be converted into heat and work once the lengthening ends. The work accumulation during *Aplysia*'s swallowing is shown in Fig. 2F (black curve). We obtain the net work produced by the muscles in a single feeding cycle, denoted by W, through the *work loop* technique, a plot of muscle force versus muscle length. For a limit-cycle behavior, the force and length return to their initial values at the end of each cycle, and therefore, a loop is constructed and the area enclosed by the loop identifies W. Fig. 3 is an example of work loops for the protractor muscle force $F_{\text{musc,pro}}$, retractor muscle force $F_{\text{musc,ret}}$, and total force F_{musc} in the default system (Fig. 2). The area inside the F_{musc} loop gives the net mechanical work done by the two buccal muscles per swallowing cycle, $W = 0.0875$ N cm.

Mechanical efficiency Energy *efficiency*, denoted by Φ, is defined as the fraction of energy used by a muscle that is converted into external work instead of heat output:

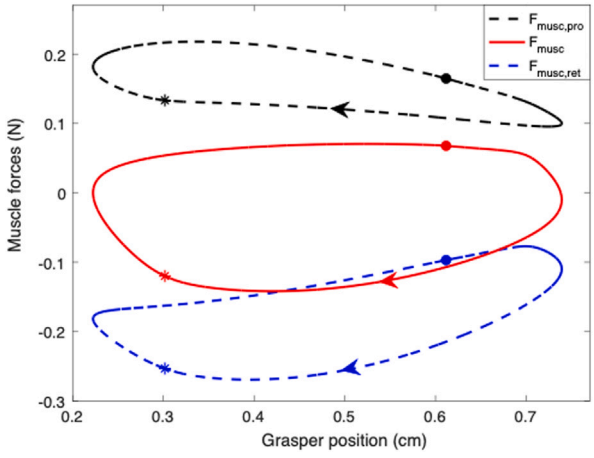

Fig. 3. Work loops of the default system, with the same parameter values as Fig. 2. Black: protractor muscle force $F_{\text{musc,pro}}$. Blue: retractor muscle force $F_{\text{musc,ret}}$. Red: total muscle force F_{musc}. Dots and stars denote the start and the end of the grasper-closed phase, respectively. Arrows mark the flow direction of the loops. The area enclosed by the F_{musc} curve (red loop) indicates the net mechanical work done by the muscles during a feeding cycle, $W = 0.0875$ N cm.

$$\Phi = \frac{W}{W + H}.$$

The heat production model and work loop analysis allow us to determine the efficiency of the buccal muscles during *Aplysia*'s swallowing behavior. For the default system without neuromodulation (see Figs. 2F and 3), per swallowing cycle, $H = 0.1696$ N cm, $W = 0.0875$ N cm, and therefore $\Phi = 0.34$. One possible role of neuromodulation is to achieve a more efficient metabolic consumption, i.e., a higher Φ. In the next

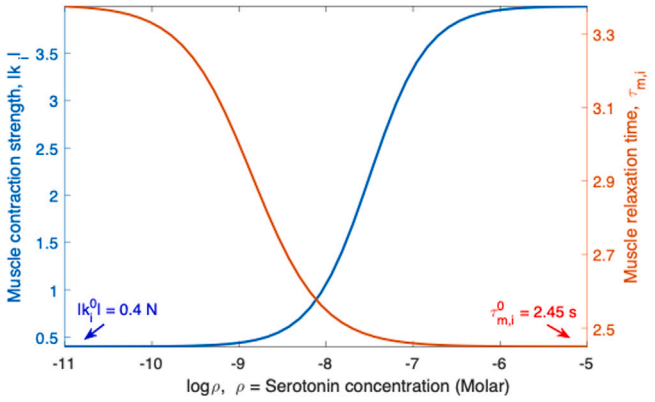

Fig. 4. Effects of the concentration of serotonin ρ on muscle contraction strength k_i (blue) and muscle relaxation time $\tau_{m,i}$ (red). The effect on the muscle contraction strength is modeled by $|k_i(\rho)| = 0.4+3.6/(1+e^{-3(\log\rho+7.5)})$, which is qualitatively similar to the 5-HT curve in Fig. 11 of Hurwitz et al. (2000). The effect on the muscle relaxation time follows $\tau_{m,i}(\rho) = 2.45 + 0.93/(1 + e^{2.5(\log\rho+8.85)})$, approximating the series of decay durations shown in Fig. 8(A2) of Hurwitz et al. (2000) and scaled appropriately to fit our model.

section, we explore how neuromodulation affects muscle contractions and efficiency.

2.3. Effects of neuromodulation

Neuromodulators can enhance muscle properties (as sketched in Fig. 1B), such as strengthening the force of muscle contractions and accelerating muscle activation and relaxation. As a consequence, the muscles' total energetic outputs may increase because of the change in their activities. In this section, we consider serotonin as the main neuromodulator and model its effects on the I2 and I3's muscular properties based on existing experimental studies.

Direct studies in Hurwitz et al. (2000) on the serotonergic and peptidergic modulation of *Aplysia*'s I2 muscle have suggested that the concentration of serotonin (ρ) has an increasing sigmoid-like effect on the muscle contraction strength (k_i), saturating at a ten-fold increase compared with the unmodulated case. At the same time, the serotonin and peptides significantly enhance the muscle's relaxation rate, especially at lower concentrations, whereas the muscle's activation rate is less sensitive to variations in the modulators' concentrations. Moreover, we note that although the rise time is much faster than the decay time when the modulation is weak, the fully modulated muscle shows a decay time approximately equal to the rise time. To account for the different effects of modulation on the muscle activation and relaxation, we modify the original neuromechanical model by separating the time constants ($\tau_{m,i}$) for different phases of the muscle contraction. See Appendices A and C for the modification details.

We assume in our model that the serotonin exerts actions that qualitatively resemble the experimental measurement on the muscular properties. Quantitatively, we approximate the effects on the muscle contraction strength and the relaxation rate with two sigmoid curves, as shown in Fig. 4. Note that at low concentrations, the serotonin has a profound effect on the muscle relaxation time but a modest effect on the contraction amplitude, which is the reverse of the response to the high concentrations. Specifically, the muscles' strength remains approximately at $k_i^0 = \pm 0.4$ N until the serotonin concentration reaches above $\rho = 10^{-8.5}$ M and starts progressively potentiating the muscles' contraction. In contrast, the acceleration effect on the muscles' relaxation is more significant at serotonin concentrations ranging from 10^{-10} to 10^{-8} M. At higher concentrations, the muscle decay duration is close to the rise duration $\tau_{m,i}^0 = 2.45$ s. Appendix C presents more details about our quantification.

Below, we combine the energetic model (Section 2.2) and neuromodulatory effects (Section 2.3) into the neuromechanical system (Section 2.1), and we examine how enhancing the modulation intensity affects the mechanical efficiency.

3. Results

We vary the concentration of serotonin and obtain the energy consumed by work and heat per swallowing movement as well as the energetic efficiency, as shown in Fig. 5. The figure suggests several insights into the role of neuromodulation in energetics, which we discuss in detail below.

3.1. Energetic plateaus

Two plateaus in the energetic values and efficiency arise, corresponding to either weak neuromodulation ($\rho < 10^{-10}$ M), which is insufficient for modulators to act, or strong neuromodulation ($\rho > 10^{-6}$ M), in which the effect of the modulators may have saturated. Moreover, the full modulation (right plateau) is advantageous over the weak modulation (left plateau) in terms of efficiency.

When the system is subjected to low concentrations of serotonin, the muscles' relaxation is affected immediately by the modulation whereas the muscles' contraction strength is initially insensitive (Fig. 4). The energetics shows notable changes until ρ reaches 10^{-10} M, at which concentration the muscle relaxation significantly accelerates and the contraction is potentiated. Another plateau occurs when the serotonin concentration exceeds 10^{-6} M, where the muscle contraction strength saturates and the relaxation time remains at the lower threshold. These two plateaus correspond, respectively, to the plateaus of the $k_i(\rho)$ and $\tau_{m,i}(\rho)$ sigmoid curves shown in Fig. 4. The right plateau illustrates the diminishing effect of modulation beyond the intermediate range. On the other hand, the left plateau suggests that the modulatory control of the muscles requires a threshold for the animal to respond to the up-regulation of serotonin.

Comparing the two plateaus in the efficiency plot (Fig. 5B), we observe that the right plateau, achieved with sufficiently high concentrations of serotonin, lies higher than the left plateau representing an inadequate amount of serotonin. This difference indicates that the fully modulated system is energetically more efficient than the unmodulated system. Higher serotonin concentrations enhance the amplitude of muscle contraction in parallel with the relaxation rate of muscle contraction, allowing the buccal muscles to generate more mechanical work with a shorter swallowing duration, which may improve the mechanical efficiency. However, this effect is not monotonic when compared with the moderately modulated system, as we discuss below.

3.2. Neuromodulatory tradeoffs

As the concentration of serotonin increases, the mechanical efficiency in Fig. 5B increases from the left plateau to a maximum (green dot) and then declines until approaching the right plateau. This trend gives rise to an optimal modulation level around $\rho^* \approx 10^{-7.78}$ M (i.e., 16.6 nM) that contributes to the maximal efficiency $\Phi^* \approx 0.532$ (under this parameter setting). For the non-plateau region where $\rho \in (10^{-10}, 10^{-6})$ M, we divide it into three sub-regions — before the optimum, around the optimum, and after the optimum, and discuss the changes in the system dynamics and energetics within each sub-region.

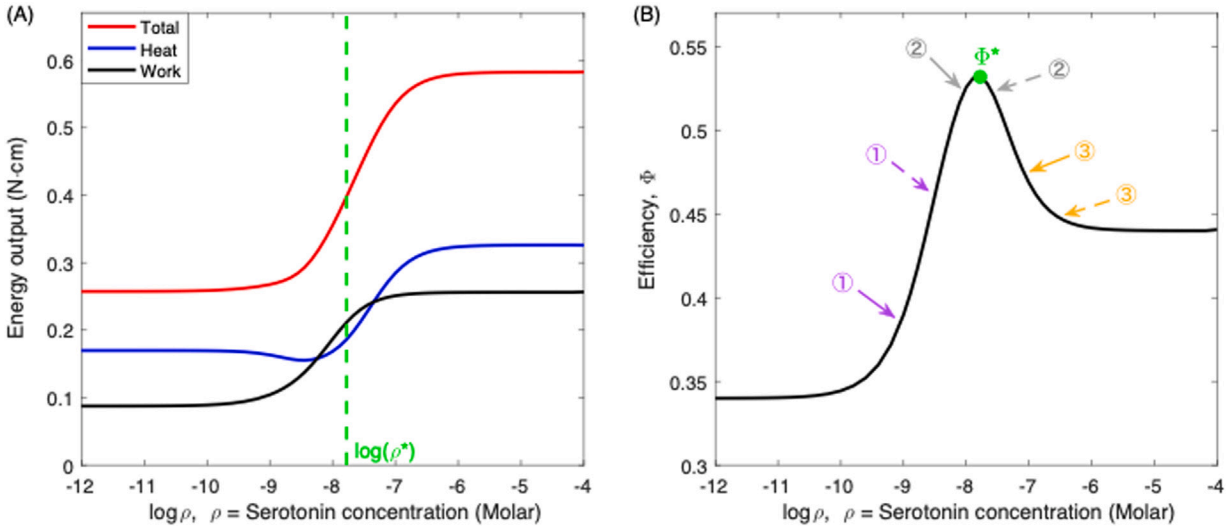

Fig. 5. Effects of serotonin concentration ρ on the energetic consumption and efficiency. **(A)**: Heat output H (blue), work output W (black), and total energy costs $W + H$ (red). **(B)**: Efficiency $\Phi = W/(W + H)$. The peak efficiency is marked in green, where $\rho^* \approx 10^{-7.78}$ M (i.e., 16.6 nM) and $\Phi^* \approx 0.532$. Each pair of arrows of the same color corresponds to the systems being compared before the optimum (magenta arrows ①, see Figs. 6, 7, 8), around the optimum (gray arrows ②, see Figs. 9, 10), and after the optimum (yellow arrows ③, see Fig. 11).

Before the optimum Consider $\rho \in (10^{-10}, 10^{-8.7})$ M. Within this range, the work output curve always lies below the heat output curve (Fig. 5A), leading to a small energetic efficiency. Nonetheless, an increased amount of serotonin promotes work generation and reduces heat production, which accounts for the rapid increase in the efficiency curve. For example, Fig. 6 compares the trajectories of two modulated systems with $\rho = 10^{-9}$ M (i.e., 1 nM, solid) and $\rho = 10^{-8.5}$ M (i.e., 3.16 nM, dashed), corresponding to the magenta arrows ① in Fig. 5B. As shown in Fig. 4, the higher concentration of serotonin shortens the muscles' relaxation time ($\tau_{m,i} = 3 \to 2.72$ s) and strengthens the muscle forces ($|k_i| = 0.44 \to 0.57$ N), consistent with the u_i- and force-trajectories in Fig. 6B, D. Consequently, both the closed and open phases are advanced (vertical magenta lines); at the same time, the stronger muscle forces pull the grasper more quickly to draw in more food during a shorter closed phase duration (panels C, D). Therefore, the mechanical work done by the muscles accumulates more rapidly (panel F), and the net work produced by the muscles after a single movement, given by the area enclosed by the F_{musc} loop shown in Fig. 7, is increased ($W = 0.1043 \to 0.133$ N cm) due to the larger forces and the greater inward movement of the seaweed.

On the other hand, the heat output is less sensitive to the change of serotonin concentration over this range of ρ (see Fig. 5A, blue curve). As shown in Fig. 6F, the two modestly modulated systems show little difference in their total heat production (blue curves, 0.1631 vs 0.1552 N cm). Fig. 8 plots time traces of each component of the heat output for the two systems. The amount of heat accumulation differs greatly from the lengthening heat during I3 protraction. Specifically, the labile heat generated by the system with stronger modulation decreases (panel B), which is however compensated by the increase in the conversion of more work to heat (panel C, consistent with Fig. 7). Hence, the overall heat production by the two systems is not significantly different. Taking both heat and work into consideration, as ρ increases, the energetic efficiency given by

$$\Phi(\rho) = \frac{W(\rho)}{W(\rho) + H(\rho)} = \frac{1}{1 + H(\rho)/W(\rho)}, \tag{1}$$

is therefore enhanced due to the significant increase of W and the small change in H.

Around the optimum Consider $\rho \in (10^{-8.7}, 10^{-7.5})$ M. The work output catches up and exceeds the heat output, resulting in an efficiency peak attained at $\rho^* \approx 10^{-7.78}$ M (16.6 nM). Then, the heat production becomes more rapid than the work, which accounts for the efficiency decline after the optimum. Compare two systems with $\rho = 10^{-8}$ M (i.e., 10 nM) and $\rho = 10^{-7.6}$ M (i.e., 25.12 nM) on the two sides of the optimum (see the gray arrows ② in Fig. 5B), as shown in Figs. 9, 10. Unlike the "before the optimum" case, where the intensified modulation profoundly shortens muscle relaxation and moderately strengthens muscle forces, here the situation is reversed, i.e., the time constant only decreases modestly whereas the muscle forces increase much more dramatically ($\tau_{m,i} = 2.55 \to 2.49$ s, $|k_i| = 1.06 \to 1.93$ N). However, the transition between closed and open phases is advanced more significantly even with the insignificant increase in the acceleration of muscle relaxation. This early transition occurs because the stronger muscle forces (Fig. 9D) due to the large increase in $|k_i|$ have a remarkable effect on accelerating the grasper movement (panel C). The proprioceptive feedback integrates the biomechanical change and then shifts the timing of the retraction pool deactivation (panel A). The mechanical work, achieved through larger forces and greater movement of muscles (panel E), is therefore significantly increased ($W = 0.1868 \to 0.2274$ N cm, black curves in panel F).

Note in these systems that the work curve lies slightly above the heat curve (see Fig. 5A and compare Figs. 6F, 9F). The strong potentiation of neuromodulators on the muscle contraction amplitude contributes to this change. Since the muscles' stretch and absorption of work becomes heat, the heat output during lengthening contraction grows in the system with stronger modulation as well (Fig. 10C). Whether the growth in the heat is comparable to the work increase determines the efficiency change. Following (1), the efficiency derivative with respect to ρ is given by

$$\Phi'(\rho) = \frac{WH}{(W + H)^2}\left(\frac{W'}{W} - \frac{H'}{H}\right),$$

where W' and H' denote the derivatives of the work and heat, respectively, with respect to ρ. Hence, the peak efficiency is attained at ρ^* when $\Phi'(\rho^*) = 0$, i.e.,

$$\frac{W'(\rho^*)}{W(\rho^*)} = \frac{H'(\rho^*)}{H(\rho^*)}.$$

That is, the relative changes in the two quantities are equivalent. In our model, increase in the neuromodulation allows the existence of a single efficiency optimum $\Phi^* \approx 0.532$ at $\rho^* \approx 10^{-7.78}$ M (16.6 nM).

After the optimum Consider $\rho \in (10^{-7.5}, 10^{-6})$ M. The enhancement of neuromodulation continues increasing the amount of heat output while the work production remains almost unchanged (Fig. 5A). Therefore,

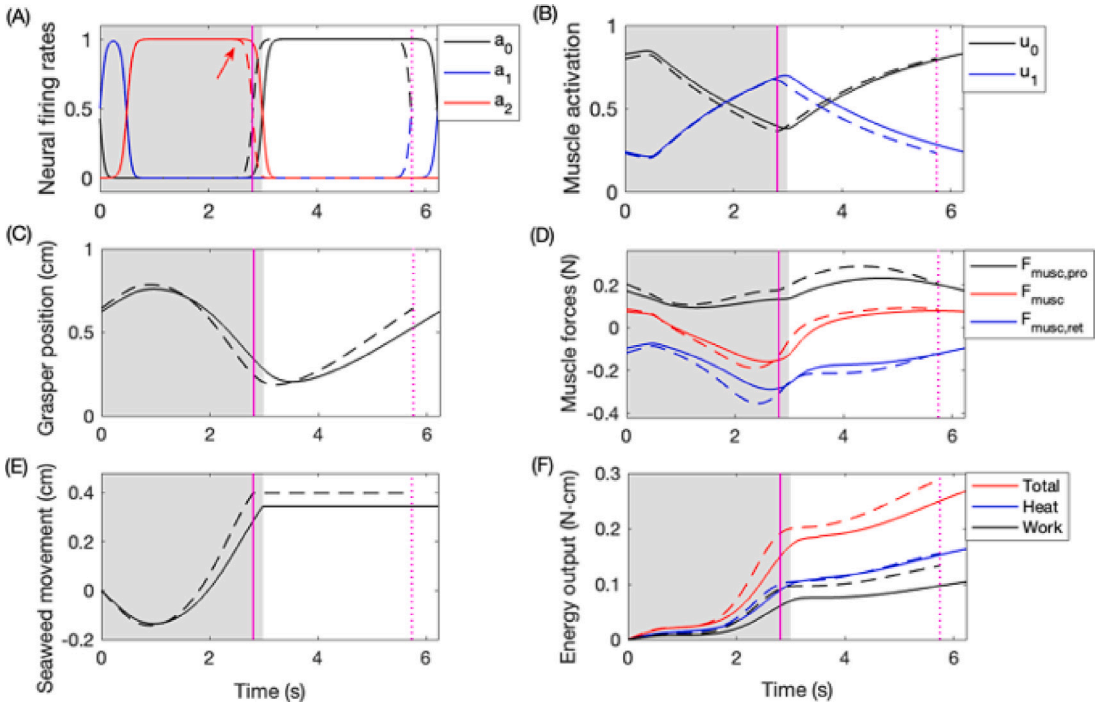

Fig. 6. Comparison of grasper trajectories prior to optimal modulation. Solid: $\rho = 10^{-9}$ M; dashed: $\rho = 10^{-8.5}$ M (Fig. 5B, magenta arrows ①). Same layout as in Fig. 2. Both systems are initiated at the start of their respective closed phase and plotted over one period. The gray shaded region represents the closed phase of the system with $\rho = 10^{-9}$ M, and the white region represents its open phase. The vertical magenta solid line denotes the transition time of the system with $\rho = 10^{-8.5}$ M out of the closed phase. The effect of the increased neuromodulation on neural pools is delayed until the transition from closed to open (panel A, red arrow). The vertical magenta dotted line denotes the end of the open phase. Both closed and open phases are advanced due to the effect of the higher serotonin concentration on accelerating muscles' relaxation (panel B). Another effect is manifested by the stronger muscle forces (panel D), which allows the system to pull in more seaweed (panels C and E) in even a shorter time. Hence, more work is done by the muscles (panel F).

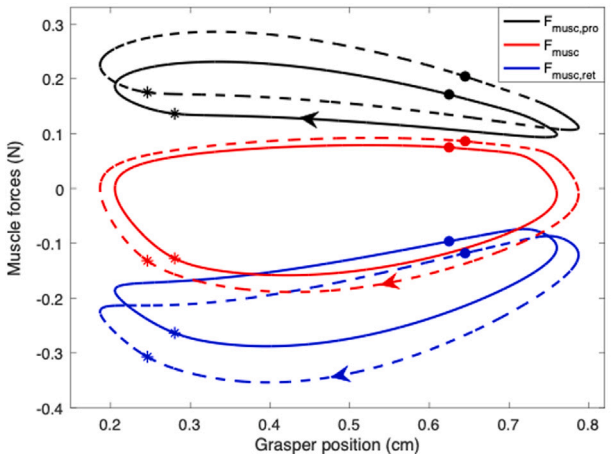

Fig. 7. Comparison of the work loops for the modulated systems with $\rho = 10^{-9}$ M (solid) and $\rho = 10^{-8.5}$ M (dashed) (the same systems as in Fig. 6). Colors and notations as in Fig. 3. The higher concentration of serotonin increases muscle forces to induce the system to produce larger retraction and protraction movements. The net work generated by the muscles within a single movement (area inside the red loops) is increased from 0.1043 N cm for $\rho = 10^{-9}$ M to 0.133 N cm for $\rho = 10^{-8.5}$ M.

the energetic efficiency decreases monotonically from the peak until reaching the right plateau (Fig. 5B). As shown in Fig. 11, we compare two systems with $\rho = 10^{-7}$ M (i.e., 100 nM) versus $\rho = 10^{-6.5}$ M (i.e., 316.23 nM), which correspond to the yellow arrows ③ in Fig. 5B. Because the muscle relaxation time remains approximately at the lower threshold ($\tau_{m,i} = 2.459$ vs 2.453 s) and the muscle contraction strength approaches the upper threshold ($|k_i| = 3.34$ vs 3.83 N) (see Fig. 4), the neural and muscle dynamics of the two systems do not show large differences. Therefore, the muscles in the two systems produce a similar amount of net mechanical work given by the area inside their almost overlapping F_{musc}-loops (cf. black curves in Fig. 11C and the red curves in Fig. 11D). On the other hand, the more modulated system generates more heat. In particular, more work is done on the contractile element during the muscles' stretch, and is converted into heat (see Fig. 11G). This greater heat production indicates that increasing neuromodulation above the optimum is not necessarily beneficial to the system's mechanical efficiency. As a consequence, the efficiency of the over-modulated system after the optimum declines (Fig. 5).

3.3. Sensitivity analysis

In order to assess the generality of the results presented in the preceding sections, we systematically vary key system parameters. Specifically, we autonomously sweep the muscle contraction strength parameter k_i and muscle relaxation rate parameter $\tau_{m,i}$ in the absence of neuromodulatory effects, with the muscle activation rate $\tau^0_{m,i}$ fixed at some specific values. Fig. 12 shows the efficiency as a function of $(\tau_{m,i}, k_i)$, with $\tau^0_{m,i} = 2.45$ or 1.5 s. In each panel, we superimpose a neuromodulation path on the contour plot, each possessing the base muscular properties including fixed $|k^0_i| = 0.4$ N (i.e., the base value of muscle contraction strength without modulation) and $\tau^0_{m,i} = 2.45$ or 1.5 s (i.e., the base value of muscle relaxation time with full modulation, which is equal to the activation time), as the modulation level ρ varies from 10^{-12} M (insufficient modulation) to 10^{-4} M (full modulation). The corresponding muscular properties, $k_i(\rho)$ and $\tau_{m,i}(\rho)$, follow the sigmoid curves shown in Fig. 4. We observe that both the modulation paths start from a low efficiency plateau, pass through higher contours to reach a peak efficiency point, and finally descend to a low plateau (but higher than the starting plateau). Their evolution

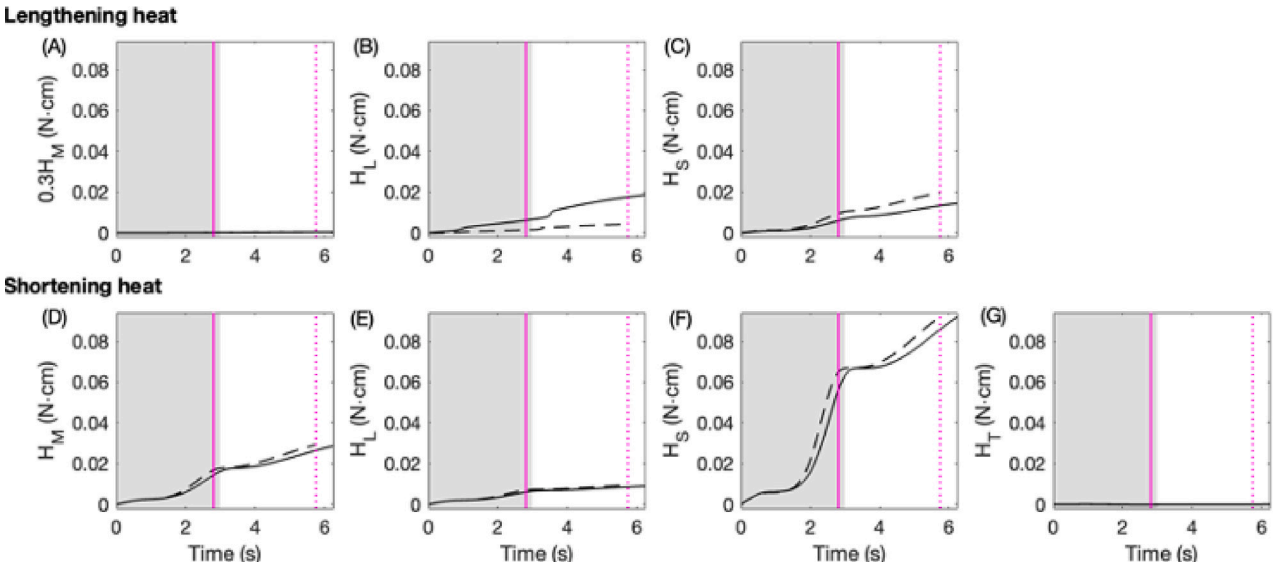

Fig. 8. Comparison of heat production for the modulated systems with $\rho = 10^{-9}$ M (solid) and $\rho = 10^{-8.5}$ M (dashed) (the same systems as in Figs. 6, 7) The gray shaded regions and the magenta lines have the same meanings as in Fig. 6. Top panels: heat generated by lengthening contraction, consisting of **(A)** stable heat, **(B)** labile heat, and **(C)** shortening heat. Bottom panels: heat generated by shortening contraction, consisting of **(D)** stable heat, **(E)** labile heat, **(F)** shortening heat, and **(G)** thermoelastic heat. Note that the end points represent the total amount of each heat component after a swallowing movement. The modulation makes a large difference in the protraction phase where the I3 muscle is stretched. The higher serotonin concentration reduces the labile heat component (panel B) while increasing the heat generated by the work done on the contractile component (panel C) during the muscles' stretch. The two changes offset each other, leading to a slight decrease in the total heat output (cf. Fig. 6F, blue curves).

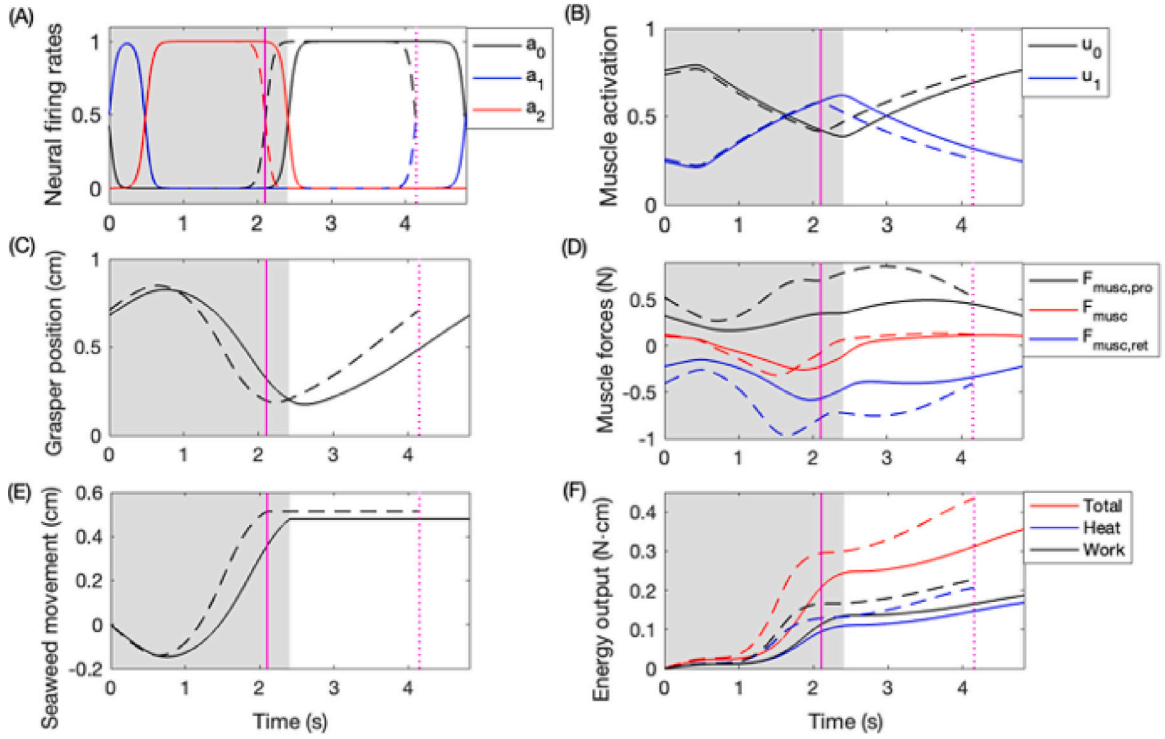

Fig. 9. Comparison of grasper trajectories around optimal modulation. Solid: $\rho = 10^{-8}$ M; dashed: $\rho = 10^{-7.6}$ M (Fig. 5B, gray arrows ②). Same layout as in Fig. 2. Both systems are initiated at the start of their respective closed phase and plotted over one period. The gray shaded region represents the closed phase of the system with $\rho = 10^{-8}$ M, and the white region represents its open phase. The vertical magenta solid line denotes the transition time of the system with $\rho = 10^{-7.6}$ M out of the closed phase. The vertical magenta dotted line denotes the end of the open phase. The higher concentration of serotonin strengthens muscle forces (panel D), which accelerates the movement of the grasper (panel C) for a longer distance (panel E). The sensory feedback propagates the biomechanical change to the neural pools and advances the timing of neural (de)activation (panel A). The muscles' work output is increased due to the larger forces and longer movement (panel F).

is consistent with the energetic plateaus and peak efficiency discussed in Section 3.1 and Section 3.2 (cf. Fig. 5).

Our analysis demonstrates the robustness of the energetic plateaus and efficiency peak against muscle property parameter variations.

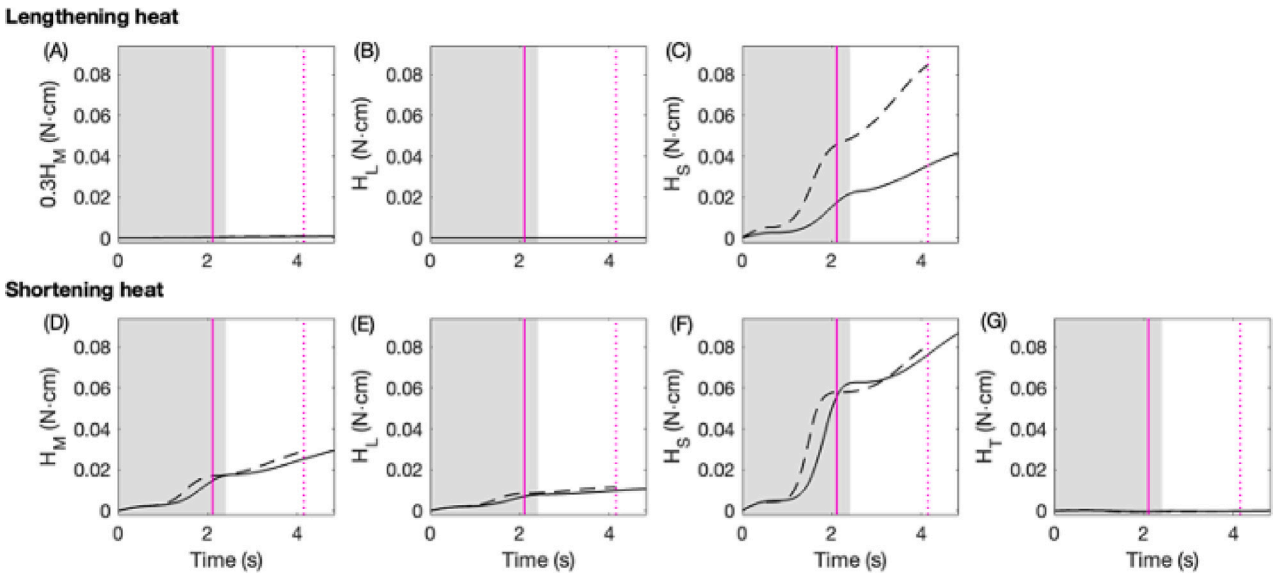

Fig. 10. Comparison of heat production for the modulated systems with $\rho = 10^{-8}$ M (solid) and $\rho = 10^{-7.6}$ M (dashed) (the same systems as in Fig. 9) The gray shaded regions and the magenta lines have the same meanings as in Fig. 9. Top panels: heat generated by lengthening contraction, consisting of **(A)** stable heat, **(B)** labile heat, and **(C)** shortening heat. Bottom panels: heat generated by shortening contraction, consisting of **(D)** stable heat, **(E)** labile heat, **(F)** shortening heat, and **(G)** thermoelastic heat. Increased neuromodulation significantly increases the "shortening heat" component during muscles' stretch (panel C).

Moreover, we find that Fig. 12 shows the globally optimal efficiency would occur for shorter muscle relaxation times that can be reached via neuromodulation. This observation emphasizes the importance of incorporating experimentally measured neuromodulatory effects into the model, as opposed to global parameter optimization without regard to biological constraints. In addition, it raises the interesting question about the evolutionary constraints on the physiology of neuromodulation.

4. Discussion

Physiological studies support the idea that neuromodulatory processes contribute to the enhancement of muscular properties controlling muscle contractions that shape multiple behaviors (Weiss et al., 1978; Hurwitz et al., 2000; Brezina et al., 2000b; Magni et al., 2009; Lu et al., 2015; Cropper et al., 2018). In contrast, there are relatively few theoretical and experimental studies on modulatory control of energy metabolism related to musculature. In this paper, we used a closed-loop neuromechanical system, based on a firing rate model of the feeding pattern generator of the marine mollusk *Aplysia californica* (Shaw et al., 2015; Lyttle et al., 2017; Wang et al., 2022), to investigate the effect of neuromodulation on tuning the system's metabolic requirements. In a nutshell, we ask: given physiological constraints, does neuromodulation lead to an optimum form of metabolic efficiency?

This work found neuromodulatory tradeoffs in the energy efficiency of *Aplysia*'s rhythmic swallowing behavior. We incorporated smooth muscle energetics and neuromodulatory effects into the original model, and determined the efficiency as a function of the animal's behavior and the neuromodulators' abundance. As the modulation level changes, we observed that two efficiency plateaus arise, with the peak efficiency attained at an intermediate modulation level (Fig. 5). The low plateau occurs when the modulation is insufficient to affect muscular properties, indicating that the modulatory control has a threshold below which the animal's behavior would not be significantly affected. The high plateau occurs when the modulation is sufficiently strong, due to saturation of its effects on muscle properties. Note that this plateau lies below the optimal efficiency, which suggests that an appropriate level of modulation must be maintained. Indeed, taking into account other energy costs, e.g., basal metabolic energy consumption, neuromodulatory regulation, and transitions between different swallowing states, excessive modulation may be inefficient and disadvantageous.

We have thus addressed our question raised above: neuromodulation does lead to the existence of a single efficiency optimum, and this optimum emerges from the effects of serotonin on the length-tension (peak force) and force-frequency (muscle relaxation time constant) of the muscles, which shape the trajectories on the energy efficiency landscape.

Consider the relative energetic costs and benefits of feeding. Studies of time budgeting of *Aplysia* in the field and the aquarium suggest that at least 75% of the time the mollusk is *not* engaged in feeding behavior (Susswein et al., 1983). To ensure adequate energy supply, the animal must obtain sufficient energy within a limited feeding time, and hence the amount of energy gained must be much greater than the energy expended as it ingests food. To the best of our knowledge, the energy expended by feeding relative to other behaviors, e.g., locomotion and reproduction, has not been measured. In contrast to locomotion and reproduction, *Aplysia*'s feeding behavior lends itself to quantitative (e.g., work loop) analysis. If we take into account energetic benefits and assume that the *Aplysia*'s sole energetic source is the seaweed it ingests, then we can quantify the energy gained, denoted by E_{gain}, to be proportional to the length of seaweed drawn in per swallow. Specifically,

$$E_{\text{gain}} = \frac{1}{50}\beta|\Delta x_r|.$$

As illustrated in Fig. 2C,E, we assume the seaweed moves together with the grasper, and Δx_r (in cm) represents the net change in the grasper position x_r during the grasper-closed phase (shaded regions in panel C), which has the same magnitude as the length of seaweed drawn in (panel E). Parameter $\beta = 0.21$ kcal/cm measures the calories of *wet* seaweed per unit length. The factor 1/50 consists of two sub-factors: (i) Carefoot (1967) found the digestion efficiency of *Aplysia punctata* on a red algae *Plocamium* in the *dry* form is about 1/5, caused by incomplete absorption of food (59%) and conversion of the absorbed food into tissues (36%); and (ii) the proportion of dry food matter (carbohydrates, protein, and fat) in the wet red algae accounts for about 1/10 of the total mass.[3] Based on these assumptions, we estimated that

[3] The calories and nutritions of wet red algae are available online at https://slism.com/calorie/109010/.

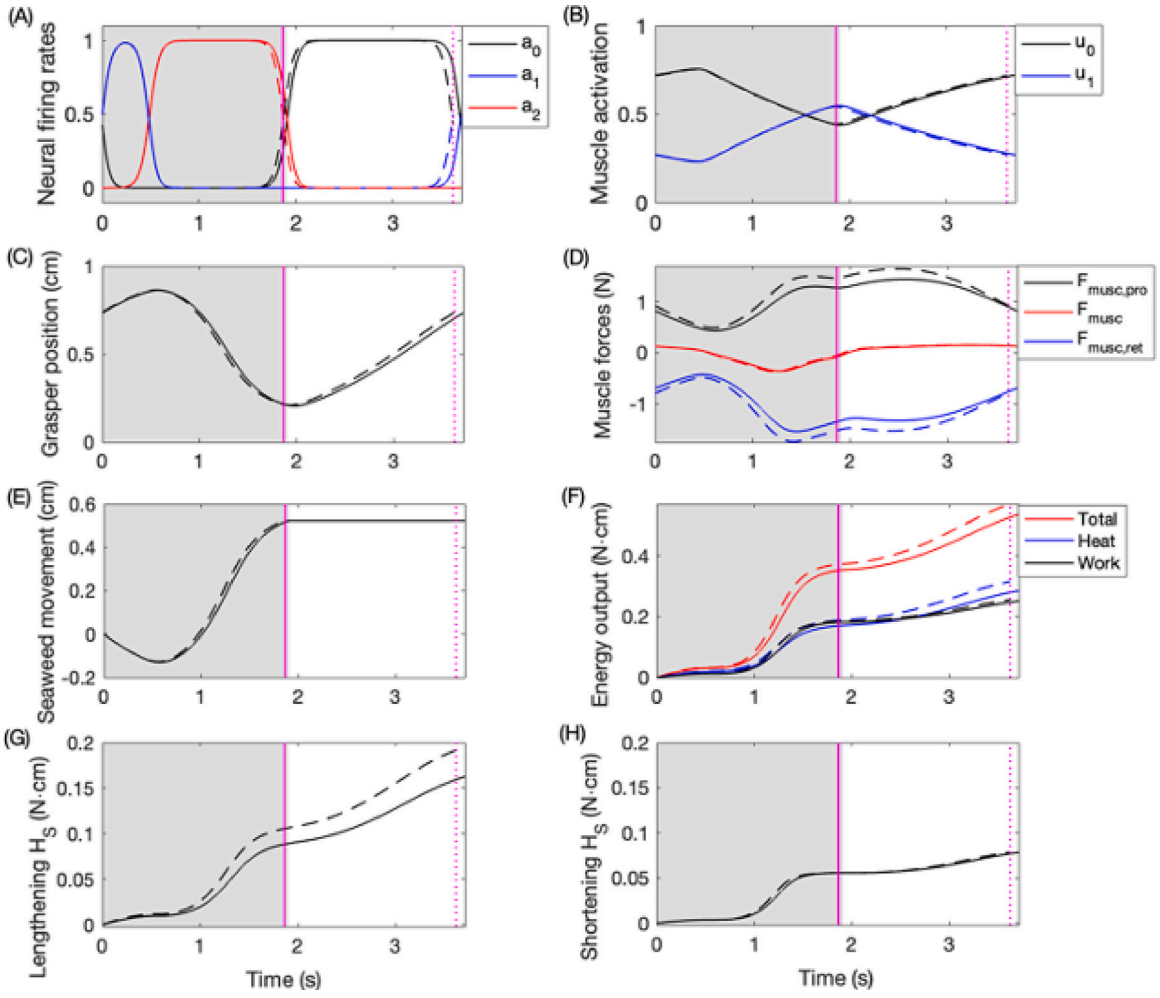

Fig. 11. Comparison of grasper trajectories above optimal modulation. Solid: $\rho = 10^{-7}$ M; dashed: $\rho = 10^{-6.5}$ M (Fig. 5B, yellow arrows ③). Panels **(A–F)** follow the same layout as in Fig. 2; **(G)**: heat generated during muscle stretch; **(H)**: heat generated during muscle contraction. Both systems are initiated at the start of their respective closed phase and plotted over one period. The gray shaded region represents the closed phase of the system with $\rho = 10^{-7}$ M, and the white region represents its open phase. The vertical magenta solid line denotes the transition time of the system with $\rho = 10^{-6.5}$ M out of the closed phase. The vertical magenta dotted line denotes the end of the open phase. Panels A–F show the same traces as in Fig. 2; panels G and H show the shortening heat component during lengthening contraction and shortening contraction, respectively. The insensitivity of the muscular properties ($\tau_{m,i}$ and k_i) to the modulation difference results in similar neural and muscle dynamics for the two systems (panels A–E), leading to a similar amount of net work generation (panel F, black curves). The heat dynamics differs (panel F, blue curves) because muscles' stronger stretch absorbs more work, which is converted into heat during lengthening contraction (panel G).

the default system (cf. Fig. 2) gains 1.3×10^{-3} kcal (i.e., 544 N cm) energy per swallowing movement, which is three orders of magnitude larger than the costs ($W + H = 0.257$ N cm). This huge difference between *Aplysia*'s energy expenditure and energy benefits per swallow is consistent with previous experimental observations.

We modeled the neuromodulation of the muscles by varying the speed and strength parameters of muscle contractions, allowing the muscles to more effectively respond to increasing mechanical load from food. Our modeling analysis is robust to variations in muscle property parameters (within reasonable ranges) that are directly subjected to modulation. Although the peak of the efficiency is sensitive to parameters as shown in sensitivity analysis (Section 3.3), the existence of the optimum is robust. Specifically, we obtained similar efficiency tradeoffs under different parameter settings, although the location and height of the peak efficiency shifted (see Fig. 12). Despite the simplicity of our model, our observations may be applied to neuromechanical systems generally, and lead to experimental tests of the role of neuromodulation in motor systems.

To test our predictions, it may be possible in a semi-intact preparation (McManus et al., 2012) to determine the levels of serotonin during swallowing by using new technology that can monitor very low levels of serotonin (Misia et al., 2024). In addition, the power stroke of swallowing, the retraction phase, is primarily mediated by the I3 and I4 muscles (Webster-Wood et al., 2020), and it might also be possible to determine the efficiency of their functions with and without serotonin modulation. The model developed in this paper suggests that there will be a physiologically determined optimum for serotonin modulation, and this could be found empirically.

The complex control of food intake and energy metabolism relies on the ability of the brain to integrate multiple forms of modulation, for instance those induced by serotonin, dopamine, and neuropeptides (Hurwitz et al., 2000; Magni et al., 2009; Oranth et al., 2018; Miller et al., 2022). We focused on serotonin as the main modulator in our model, because serotonin is released by the metacerebral cells (MCCs) whose modulatory influences are exerted both centrally on the nervous system as well as peripherally on muscles (Weiss and Kupfermann, 1976; Weiss et al., 1978; Magni et al., 2009; Celada et al., 2013; O'Mahony et al., 2015; Yabut et al., 2019). Centrally, the effects on neural circuit properties include regulating ongoing neural activity and varying the release of other neurotransmitters (Daubert and Condron, 2010; Celada et al., 2013). Peripherally, the muscles are modulated in a manner that enhances the rate of relaxation and the force of contraction (Brezina and Weiss, 2000; Brezina et al., 2000a,b). During motor behaviors, most of the energy is spent by muscle activation

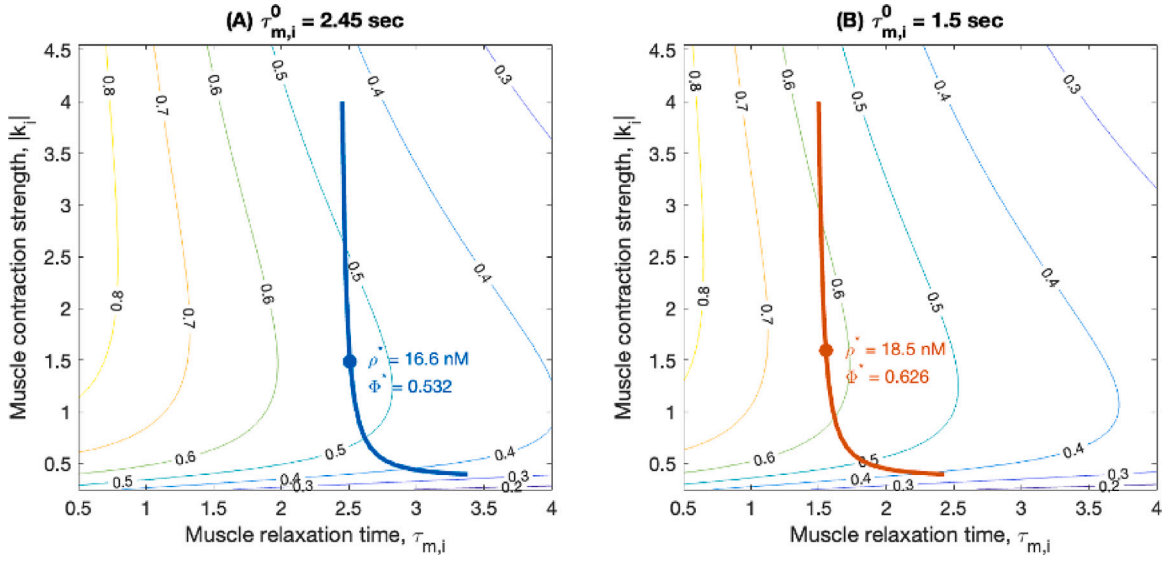

Fig. 12. Efficiency levels as muscle contraction strength $|k_i|$ and relaxation time $\tau_{m,i}$ are independently varied (in the absence of neuromodulation), with the muscle activation time $\tau^0_{m,i}$ fixed at **(A)** 2.45 s or **(B)** 1.5 s. Each contour line is labeled with its efficiency level. In each panel, the superimposed thick curve plots the modulation path with base values $|k^0_i|$ = 0.4 N, $\tau^0_{m,i}$ = 2.45 or 1.5 s, and serotonin concentration ρ varied. The serotonin concentration starts at picomolar concentrations ($\rho = 10^{-12}$ M) at the low end of each path up to almost millimolar ($\rho = 10^{-4}$ M) at the high end. An optimum at intermediate concentrations for each path is observed, consistent with the energetic plateaus and neuromodulatory tradeoffs shown in Fig. 5. The solid dot on each path indicates the optimum neuromodulation point, labeled with the value of ρ^* (in nM) and the peak efficiency Φ^*. Note that as $\tau^0_{m,i}$ decreases, the contours shift to the left, indicating that the muscular time constant property has a larger effect on the efficiency pattern than the peak force property does.

rather than activation of the nervous system (Tesch et al., 1986; Baker et al., 2010; Hargreaves and Spriet, 2020). Therefore, we focused on biomechanics and muscle metabolism subjected to peripheral modulation from serotonin, and neglected the modulator's effect on central neuronal properties.

However, the neural activity and release of neurotransmitters associated with neuromodulation do require energy. For example, energy consumption within the neural circuits can directly shape the activity itself and influence motor performance (Burroni et al., 2017), potentially modulating the efficiency of the neuromechanical system. In addition, neurotransmitter release is also an energy-demanding process, including the synthesis of neurotransmitters in presynaptic neurons, synaptic vesicle loading and recycling, and the activation of postsynaptic receptors, all of which require a significant energy cost in the brain (Attwell and Laughlin, 2001; Attwell and Gibb, 2005; Rangaraju et al., 2014). Therefore, incorporating these factors into future models will be an important step towards understanding the full scope of energetic tradeoffs in a neuromechanical system.

Our paper proposed an empirically based model to predict the mechanical energetic output of *Aplysia*'s buccal muscles for a wide range of contraction properties. Our smooth muscle energetics model is based on a modified Hill-type model (Hill, 1938; Lichtwark and Wilson, 2005), and our neuromodulation model is a quantification of the previous experimental studies on serotonergic and peptidergic modulation of *Aplysia*'s protractor muscle (I2) (Hurwitz et al., 2000). To the best of our knowledge, modeling studies of neuromuscular systems have not investigated the relationship between neuromodulatory mechanisms and energetic budgets. Our study presented a modeling framework for making predictions about the mechanics and energetics of a muscle given information about the specific muscle.

This work extended *single* parameter analysis of earlier work to a *multi*-parameter analysis. Methodologically, Wang et al. (2021) established a general *variational* (sometimes called *linearized*) tool for studying how a change in a single parameter affects the system dynamics, which provides a mathematically grounded numerical quantification for many biological phenomena including fitness (Wang et al., 2022), homeostasis (Yu and Thomas, 2022), and robustness (Yu and Thomas, 2024). In Wang et al. (2022), they applied the variational tool to the same system modeling *Aplysia*'s swallowing behavior in order to understand the effect of changing seaweed load on the system's performance and robustness. Here for our sensitivity analysis (Fig. 12), we varied the muscle contraction force and relaxation rate simultaneously to study the system's energetic response to parameter variations. Considering the coordinated change in *multiple* parameters, our work provides a motivating example for studying multi-factor sensitivity and points out a possible future direction for further methodological development.

In the current study, we only considered the effect of changing muscle properties (muscle contraction strength and relaxation time) on the energy efficiency landscape and did not consider the effect of changing environments. Given that the relationship between muscle force and grasper position depends on seaweed load (F_{sw}), we performed a neuromodulation analysis while varying F_{sw}, as shown in Fig. 13. We observed similar efficiency plateaus and optima across the range of F_{sw} that gives rise to stable swallowing behavior, indicating that the contextual variable in our model does not qualitatively modify the efficiency landscape.

In contrast to the relaxation rate, the activation rate of *Aplysia*'s buccal muscles is insensitive to neuromodulatory innervation, as shown experimentally in Hurwitz et al. (2000). In the model, we set the activation time $\tau^0_{m,i}$ fixed at 2.45 s (the literature value from Shaw et al. (2015), Lyttle et al. (2017), Wang et al. (2022)) in all systems presented (Figs. 2, 5, 6, 9, 11, 12A), except for Fig. 12B where $\tau^0_{m,i}$ = 1.5 s to show the robustness of the energetic tradeoffs against parameter variations. On the one hand, we chose a smaller value of $\tau^0_{m,i}$ because the efficiency levels increase with the acceleration of muscle contractions (see Fig. 12A). On the other hand, in real life, a wide range of environmental conditions, such as temperature (Zhurov and Brezina, 2005), medium (Butler et al., 1983), and stimulations (Abbott and Lowy, 1958), may or may not affect muscular properties and physiological outputs. For instance, Zhurov and Brezina (2005) showed that increasing temperature does not change the muscle contraction shape, in that the modulatory effects and modulator release have opposite responses to temperature variations, the combination of which allows the muscle to maintain a stable output. Our modeling study, by further incorporating dynamic external conditions and performing parameter manipulations, has the potential to study the system's resilience or

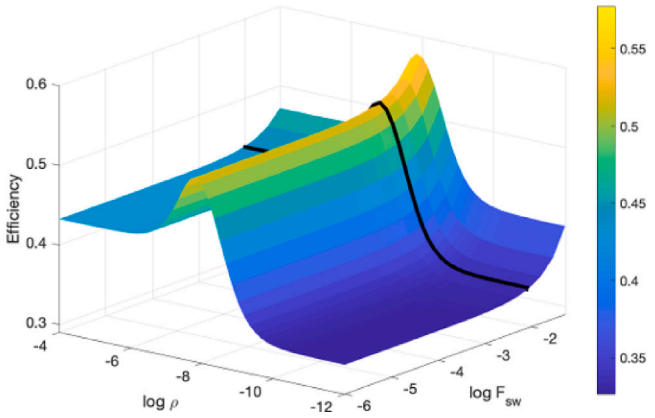

Fig. 13. Effects of serotonin concentration ρ on the energy efficiency with changing seaweed force F_{sw}. Black curve corresponds to the default system with $F_{sw} = 0.01$ N (cf. Fig. 5B). Similar plateaus and optima arise in response to different values of F_{sw}, which are relatively insensitive to the change of F_{sw}.

vulnerability to temperature as well as other external conditions.

To scale the total neuromodulated muscle forces, represented by k_i^0 (in Newtons), we were guided by the data in Hurwitz et al. (2000). That study measured total muscle contraction, and since the previous studies have shown that the force–velocity property of the I2 muscle might reduce the total force it generates (Yu et al., 1999), we applied a scaling factor to k_i^0 to the systems studied (see Appendix C) and swept the size of the scaling factor for parameter sensitivity analysis (see Fig. 12). In future studies, it would be worthwhile to measure the effects of neuromodulation on the isometric forces versus the force–velocity property.

In the present model, we considered serotonergic modulation as a proxy for neuromodulation in general, since increased concentration of serotonin increases muscle contraction strength and relaxation rate. In contrast, some other types of modulation may impose distinct and/or more complex effects on muscle properties (Weiss et al., 1992; Evans et al., 1999; Hurwitz et al., 2000). For example, while myomodulin-a (MMa) increases I2 muscle relaxation rate, it potentiates the amplitude of muscle contractions at low concentrations and depresses muscle contractions at high concentrations (Hurwitz et al., 2000). Therefore, the location of the efficiency optimum mediated by MMa may be different. Moreover, the interaction between multiple modulators could also play a significant role on the overall modulatory effect. Considering the effect of serotonin in conjunction with MMa, the optimum point may be pushed towards lower concentrations to reduce the negative effect of high-concentration MMa on muscle strength. In addition, Weiss et al. (1992) also showed that "peptides modify the relationship between muscle contraction amplitude and relaxation rate so as to maintain optimal motor output when the intensity and frequency of feeding behavior change." Some peptides potentiate muscle contractions while others reduce the contractions, and their combined actions are important to maintain proper feeding behavior (Weiss et al., 1992). In the future, including different modulators and their interactions would be expected to change our results quantitatively, but we expect our qualitative observations and insights to remain similar.

Finally, Sutton et al. (2023) suggested that in a quasi-static system underlying small locomoting animals (e.g., stick insects), neuromodulation might not compromise stability but might nevertheless improve efficiency. Here, we found an efficiency enhancement in *Aplysia* that is consistent with their study. In Fig. 5, for example, the serotonergic input always raises the efficiency level compared with the unmodulated situation, although the overly high concentrations of serotonin may reduce the efficiency from the optimum occurring at an intermediate concentration. In contrast to quasi-static systems, kinetic systems for large locomoting animals (e.g., horses) might show efficiency declines (Sutton et al., 2023). Although we do not pursue these examples here, we do not foresee any fundamental difficulty applying a similar modeling framework to these cases.

CRediT authorship contribution statement

Zhuojun Yu: Writing – original draft, Writing – review & editing, Visualization, Software, Methodology, Investigation, Formal analysis. **Yangyang Wang:** Writing – review & editing, Visualization, Validation, Supervision, Methodology, Investigation, Funding acquisition, Formal analysis, Conceptualization. **Peter J. Thomas:** Writing – review & editing, Visualization, Validation, Supervision, Methodology, Investigation, Funding acquisition, Formal analysis, Conceptualization. **Hillel J. Chiel:** Writing – review & editing, Visualization, Validation, Supervision, Methodology, Investigation, Funding acquisition, Formal analysis, Conceptualization.

Declaration of competing interest

The authors declare that they have no known competing financial interests or personal relationships that could have appeared to influence the work reported in this paper.

Acknowledgments

This work was supported in part by (1) National Institutes of Health BRAIN Initiative grant, United States RF1 NS118606-01; (2) the National Science Foundation, United States under Grant No. DMS-1929284 while the authors were in residence at the Institute for Computational and Experimental Research in Mathematics in Providence, RI, during the program; (3) NIH/NIDA R01DA057767, as part of the NSF/NIH/DOE/ANR/BMBF/BSF/NICT/
AEI/ISCIII Collaborative Research in Computational Neuroscience Program; and (4) the Oberlin College Department of Mathematics.

Appendix A. Neuromechanical model

The model we consider is adapted from Shaw et al. (2015), Lyttle et al. (2017), and Wang et al. (2022). The equations are

$$\frac{da_0}{dt} = \frac{1}{\tau_a}(a_0(1 - a_0 - \gamma a_1) + \mu + \epsilon_0(x_r - \xi_0)\sigma_0),$$
$$\frac{da_1}{dt} = \frac{1}{\tau_a}(a_1(1 - a_1 - \gamma a_2) + \mu + \epsilon_1(x_r - \xi_1)\sigma_1),$$
$$\frac{da_2}{dt} = \frac{1}{\tau_a}(a_2(1 - a_2 - \gamma a_0) + \mu + \epsilon_2(x_r - \xi_2)\sigma_2),$$
$$\frac{du_0}{dt} = \frac{1}{\tau_{m,0}}((a_0 + a_1)u_{\max} - u_0),$$
$$\frac{du_1}{dt} = \frac{1}{\tau_{m,1}}(a_2 u_{\max} - u_1),$$
$$\frac{dx_r}{dt} = \frac{1}{b_r}(F_{\text{musc}}(u_0, u_1, x_r) + rF_{\text{sw}}).$$

The neural variables a_0, a_1, and a_2 represent the firing rates of the protraction-open, protraction-closed, and retraction neural pools, respectively. The firing rates must be nonnegative, inducing three hard boundaries for the model dynamics:

$$\Sigma_0 = \{a_0 = 0\}, \quad \Sigma_1 = \{a_1 = 0\}, \quad \Sigma_2 = \{a_2 = 0\}.$$

The biomechanical system involves muscle dynamics, represented by muscle activation variables u_0 for the I2 muscle and u_1 for the I3 muscle, and the grasper position denoted as x_r. We make some modifications from the original model. For the two muscles, we distinguish their muscle activation/relaxation time parameters $\tau_{m,i}$. Studies in Hurwitz et al. (2000) suggested that the serotonergic and peptidergic

Table 1
Model parameters.

Parameter	Description	Value	Unit	Reference
γ	inhibition strength from next neural pool	2.4	none	Shaw et al. (2015)
μ	neural pool intrinsic excitation	10^{-6}	none	Wang et al. (2022)
ϵ_i	sensory feedback strength to a_i pool	10^{-4}	none	Wang et al. (2022)
ξ_0	proprioceptive neutral position for a_0 pool	0.5	none	Shaw et al. (2015)
ξ_1	proprioceptive neutral position for a_1 pool	0.5	none	Shaw et al. (2015)
ξ_2	proprioceptive neutral position for a_2 pool	0.25	none	Shaw et al. (2015)
σ_0	sign of proprioceptive input to a_0 pool	−1	none	Shaw et al. (2015)
σ_1	sign of proprioceptive input to a_1 pool	1	none	Shaw et al. (2015)
σ_2	sign of proprioceptive input to a_2 pool	1	none	Shaw et al. (2015)
τ_a	neural pool time constant	0.05	s	Shaw et al. (2015)
$u_{\max}$	maximum muscle activation	1	none	Shaw et al. (2015)
$\tau^0_{m,0}$	unmodulated I2 activation time constant	2.45	s	Yu et al. (1999)
$\tau^0_{m,1}$	unmodulated I3 activation time constant	2.45	s	Yu et al. (1999)
b_r	grasper damping time constant	0.4	N s cm^{-1}	Lyttle et al. (2017)
c_0	position of shortest length for I2	1	cm	Shaw et al. (2015)
c_1	position of center of I3	1.1	cm	Shaw et al. (2015)
w_0	maximal effective length of I2	2	cm	Shaw et al. (2015)
w_1	maximal effective length of I3	1.1	cm	Shaw et al. (2015)
k^0_0	unmodulated strength and direction of I2	0.4	N	Shaw et al. (2015), modified
k^0_1	unmodulated strength and direction of I3	−0.4	N	Shaw et al. (2015), modified
F_{sw}	force on the seaweed resisting ingestion	0.01	N	Shaw et al. (2015)
G	Hill's constant	5	none	Abbott and Lowy (1958)
K_t	buccal muscle stiffness	5	N m^{-1}	Yu et al. (1999)

Table 2
Effect of MMa on the decay time of I2 contraction, estimated from Hurwitz et al. (2000).

MMa concentration (M)	$\le 10^{-10}$	3×10^{-10}	10^{-9}	3×10^{-9}	10^{-8}	$\ge 10^{-7}$
Decay duration (s)	4.3	3.7	2.5	1.5	0.7	0.3

modulation does not have a significant effect on the activation time of the I2 muscle but does on the relaxation time. Therefore, we assume that when u_i increases $\tau_{m,i}$ remains constant (denoted by $\tau^0_{m,i}$) regardless of the neuromodulation level and that when u_i decreases the value of $\tau_{m,i}$ is determined by the modulation level given by Eq. (7).

The grasper movement is controlled by the net muscle force exerted by the muscles, i.e.,

$$F_{\text{musc}}(u_0,u_1,x_r) = F_{\text{musc,pro}} + F_{\text{musc,ret}} = k_0\phi\left(\frac{c_0-x_r}{w_0}\right)u_0 + k_1\phi\left(\frac{c_1-x_r}{w_1}\right)u_1.$$

The function ϕ is the effective length-tension curve for the muscle forces, given by

$$\phi(x) = -\frac{3\sqrt{3}}{2}x(x-1)(x+1).$$

Note that the strength of muscle contraction k_i is subjected to neuromodulation, given by Eq. (6). The grasper is also pulled by an external force F_{sw} applied by the seaweed, which is at work only when the grasper is closed on the seaweed, as suggested by the indicator $r \in \{0,1\}$. The closing and opening of the grasper is assumed to be determined by the activation of neural variables: the grasper is closed when $a_1+a_2 \ge 0.5$ and open when $a_1+a_2 < 0.5$. The physical meanings, values, and units of all the parameters are listed in Table 1.

Appendix B. Smooth muscle energetics

To capture the heat production, we adopt a modified Hill-type muscle model (Hill, 1938; Lichtwark and Wilson, 2005). The heat output from a muscle depends on crossbridge activation level (Act), velocity of the contractile component (V_{CE}), the time relative to the start of the train of stimulation (t) and the force produced by the muscle (P). Numerically, an estimate of Act is given by

$$\text{Act} = P/P',$$

where P' is the maximum isometric force P_0 scaled for the instantaneous muscle velocity. In Yu et al. (1999), the relation between P' and V_{CE} of *Aplysia*'s I2 muscle is modeled as

$$P' = \begin{cases} P_0\left(1+\dfrac{0.61}{1-0.038/(V_{\text{CE}}/V_{\max})}\right), & \text{lengthening } (V_{\text{CE}}<0), \\ P_0\left(\dfrac{1}{1+10.8(V_{\text{CE}}/V_{\max})}\right), & \text{shortening } (V_{\text{CE}}>0), \end{cases} \tag{2}$$

where $V_{\max}$ is the maximum shortening velocity.[4]

During muscle shortening ($V_{\text{CE}} > 0$), the rate of heat production can be divided into four distinct functions (f_i) of heat production, which sum to give the overall heat rate (Lichtwark and Wilson, 2005):

$$\frac{dH}{dt} = \frac{dH_M}{dt} + \frac{dH_L}{dt} + \frac{dH_S}{dt} + \frac{dH_T}{dt} = f_1(\text{Act}) + f_2^S(\text{Act},t) + f_3^S(\text{Act},V_{\text{CE}}) + f_4^S(P), \tag{3}$$

where the superscript in f_i^S denotes shortening. Here, H_M is termed the 'stable' heat, H_L the 'labile' heat, H_S the 'shortening' heat, and H_T the 'thermoelastic' heat. Specifically, the stable heat rate can be approximated by a constant in the range of $a\times b$, the product of Hill's force–velocity constants,

$$\frac{dH_M}{dt} = f_1(\text{Act}) = \text{Act}\left(\frac{V_{\max}}{G^2}\right),$$

where $G = P_0/a$ is a constant. The labile heat is controlled by the stable heat rate:

$$\frac{dH_L}{dt} = f_2^S(\text{Act},t) = 0.8\frac{dH_M}{dt}e^{-0.72t} + 0.175\frac{dH_M}{dt}e^{-0.022t}.$$

The shortening heat rate is approximated to a linear relationship with respect to the velocity of the contractile element:

$$\frac{dH_S}{dt} = f_3^S(\text{Act},V_{\text{CE}}) = \text{Act}\left(\frac{V_{\text{CE}}}{G}\right).$$

The thermoelastic heat accounts for the heat absorbed by the muscle, which is proportional to the rate of force production, given by

$$\frac{dH_T}{dt} = f_4^S(P) = -0.014\frac{dP}{dt}.$$

[4] A sign error in the original paper (Yu et al., 1999) has been corrected.

During muscle lengthening ($V_{CE} < 0$), the heat rate can be approximated with the following equation:

$$\frac{dH}{dt} = 0.3\frac{dH_M}{dt} + \frac{dH_L}{dt} + \frac{dH_S}{dt} = 0.3 f_1(\text{Act}) + f_2^L(\text{Act}, P) + f_3^L(V_{CE}, P),$$

where the superscript in f_i^L denotes lengthening. The first term accounts for 30% of the stable heat used for activating the muscle; the second term represents an exponential decay of the rate of energy production as the lengthening velocity increases, scaled by activation; the last term results from the work done on the contractile component during stretch, which is converted to heat on a short time scale. Specifically,

$$f_2^L(\text{Act}, P) = 0.7\frac{dH_M}{dt} e^{-8\left(\frac{P}{\text{Act}}-1\right)}, \qquad f_3^L(V_{CE}, P) = PV_{CE}.$$

If parameters V_{max}, G, P_0, and the force–velocity relation (2) are given, the above model of heat production, with the muscle contraction force P and instantaneous velocity V_{CE} of the contractile element obtained from the swallowing dynamics, can be applied. Based on the byssus retractor muscle of *Mytilus*, we set $G = 5$ (Abbott and Lowy, 1958). In our swallowing model, the muscle contraction force $P = F_{musc,pro}$, $P_0 = k_0$ for I2 and $P = |F_{musc,ret}|$, $P_0 = |k_1|$ for I3. We assume that a muscle–tendon unit (MTU) consists of the contractile element (CE) in series with a series elastic element (SEE), i.e.,

$$L_{MTU} = L_{CE} + L_{SEE}. \tag{4}$$

Given the instantaneous muscle force, it is possible to calculate the length of the elastic element as follows:

$$P = K_t(L_{SEE} - L_{st}), \tag{5}$$

where K_t is the stiffness and L_{st} is the maximal length at which the element exerts no force (slack length). We assume that the tendon slack length L_{st} remains constant as the muscle–tendon contracts. Then, by Eqs. (4) and (5), the velocity of the contractile component is given by

$$V_{CE} = V_{MTU} - \frac{1}{K_t}\frac{dP}{dt}.$$

During *Aplysia*'s swallowing, we assume that the muscle–tendon has the same velocity magnitude as the grasper:

$$|V_{MTU}| = |v_{x_r}| = |dx_r/dt|.$$

Specifically, the protractor muscle (I2) and the retractor muscle (I3) act as antagonists throughout the process, as indicated in Fig. 1A. In the protraction-open phase, the grasper is protracted, and the I2 muscle undergoes shortening while the I3 muscle is stretched. Then the protraction-closed phase follows, during which the grasper continues protracting a small distance by the contracted I2 muscle. In the retraction phase, the grasper is retracted by the actively contracted I3 muscle, and the I2 muscle is correspondingly stretched. Therefore, when the grasper is moved backward ($v_{x_r} < 0$) during the retraction phase, the I2 is stretched ($V_{MTU,pro} < 0$) and I3 is shortened ($V_{MTU,ret} > 0$); when the grasper is moved forward ($v_{x_r} > 0$) during the protraction phase, the contraction directions are opposite. The maximum velocity V_{max} is taken as the maximum magnitude of V_{CE} during a single feeding cycle.

Appendix C. Effects of neuromodulation

This section presents the quantitative effect of serotonin on muscle properties, including muscle contraction strength and activation time, based on existing experimental data.

- **Muscle contraction strength**
  In Hurwitz et al. (2000), by varying the concentration of serotonin (from 10^{-9} to 10^{-5} M), the authors showed a direct effect of serotonin on *Aplysia*'s I2 muscle, with a ten-fold increase in the muscle contraction amplitude and a sigmoid-like dependence as suggested in their Fig. 11. The sigmoid relation between the concentration of serotonin ρ and muscle contraction strength k_i can be approximated by the following function:

$$k_i(\rho) = k_i^0 + \frac{9k_i^0}{1 + e^{-3(\log\rho + 7.5)}}, \tag{6}$$

  where k_i^0 represents the original muscle contraction strength without modulation. Here we take $k_0^0 = 0.4$ N and $k_1^0 = -0.4$ N.

- **Muscle activation time**
  Hurwitz et al. (2000) also studied the relaxation rate of muscle contraction in response to serotonergic and peptidergic modulation, showing that the two forms of modulation both profoundly enhance the relaxation rate. The I2 activation and relaxation durations at different concentrations of the MMa peptide were measured. At low concentrations ranging from 3×10^{-10} to 10^{-8} M, in which the actions of serotonin are similar to the MMa, the decay durations are listed in Table 2 (estimated from Fig. 8(A2) in Hurwitz et al. 2000).[5] Moreover, we set the upper threshold of the decay duration to be 4.3 s when the MMa concentration is below 10^{-10} M and the lower threshold to be 0.3 s when the MMa concentration is above 10^{-7} M. The data series in Table 2 can be approximated by the following sigmoid function:

$$\tau_{decay}(\rho) = \alpha\left(0.07 + \frac{0.93}{1 + e^{2.5(\log\rho + 8.85)}}\right) + \beta, \tag{7}$$

  where $\alpha = 4.07$ and $\beta = 0$ for the Hurwitz's data series and can be scaled such that the durations fall within an appropriate range. Moreover, note that the modulators have an insignificant effect on the rise time of the I2 contraction, and that the decay duration in the fully modulated case is close to the rise duration (see Figs. 8(A2,B2), 9B, 10B in Hurwitz et al. 2000).
  In our nominal model, we assume that the rise time of the muscles' contraction is maintained at $\tau_{m,i}^0 = 2.45$ s, the value given in Shaw et al. (2015), Lyttle et al. (2017), Wang et al. (2022). To adjust the muscle relaxation time parameter $\tau_{m,i}$ to be consistent with the experimental observations, we assume that when the muscle contraction decays, the relation of $\tau_{m,i}$ with the concentration of serotonin is qualitatively similar to the sigmoid relation (7). Specifically, $\alpha = 1$ and $\beta = 2.38$, which guarantees that the fully modulated decay duration is equal to $\tau_{m,i}^0$, the rise duration. The sensitivity of the energetic efficiency to the values of $\tau_{m,i}^0$ is discussed in Section 3.3.

References

Abbott, B., Lowy, J., 1958. Contraction in molluscan smooth muscle. J. Physiol. 141 (3), 385.

Attwell, D., Gibb, A., 2005. Neuroenergetics and the kinetic design of excitatory synapses. Nature Rev. Neurosci. 6 (11), 841–849.

Attwell, D., Laughlin, S.B., 2001. An energy budget for signaling in the grey matter of the brain. J. Cereb. Blood Flow & Metab. 21 (10), 1133–1145.

Aubert, X., Hill, A., 1956. Le couplage énergétique de la contraction musculaire (Ph.D. thesis). UCL-Université Catholique de Louvain.

Baguet, F., Gillis, J., 1967. The respiration of the anterior byssus refractor muscle of *Mytilus edulis* (ABRM) after a phasic contraction. J. Physiol. 188 (1), 67–82.

Baker, J.S., McCormick, M.C., Robergs, R.A., et al., 2010. Interaction among skeletal muscle metabolic energy systems during intense exercise. J. Nutr. Metab. 2010.

Brezina, V., Orekhova, I.V., Weiss, K.R., 2000a. The neuromuscular transform: the dynamic, nonlinear link between motor neuron firing patterns and muscle contraction in rhythmic behaviors. J. Neurophysiol. 83 (1), 207–231.

Brezina, V., Orekhova, I.V., Weiss, K.R., 2000b. Optimization of rhythmic behaviors by modulation of the neuromuscular transform. J. Neurophysiol. 83 (1), 260–279.

Brezina, V., Weiss, K.R., 2000. The neuromuscular transform constrains the production of functional rhythmic behaviors. J. Neurophysiol. 83 (1), 232–259.

[5] The effect of 5-HT (serotonin) on the muscle relaxation rate was only shown at 10^{-8} M (cf. Fig. 10B of Hurwitz et al. 2000).

Burroni, J., Taylor, P., Corey, C., Vachnadze, T., Siegelmann, H.T., 2017. Energetic constraints produce self-sustained oscillatory dynamics in neuronal networks. Front. Neurosci. 11, 80.
Butler, T.M., Siegman, M., Mooers, S.U., 1983. Chemical energy usage during shortening and work production in mammalian smooth muscle. Am. J. Physiol. Cell Physiol. 244 (3), C234–C242.
Carefoot, T.H., 1967. Growth and nutrition of *Aplysia punctata* feeding on a variety of marine algae. J. Mar. Biol. Assoc. UK 47 (3), 565–589.
Carefoot, T.H., 1970. A comparison of absorption and utilization of food energy in two species of tropical *Aplysia*. J. Exp. Mar. Biol. Ecol. 5 (1), 47–62.
Celada, P., Puig, M.V., Artigas, F., 2013. Serotonin modulation of cortical neurons and networks. Front. Integr. Neurosci. 7, 25.
Chiel, H.J., Beer, R.D., 1997. The brain has a body: adaptive behavior emerges from interactions of nervous system, body and environment. Trends Neurosci. 20 (12), 553–557.
Cropper, E.C., Brezina, V., Vilim, F.S., Harish, O., Price, D.A., Rosen, S., Kupfermann, I., Weiss, K.R., 1994. FRF peptides in the ARC neuromuscular system of *Aplysia*: purification and physiological actions. J. Neurophysiol. 72 (5), 2181–2195.
Cropper, E.C., Jing, J., Vilim, F.S., Weiss, K.R., 2018. Peptide cotransmitters as dynamic, intrinsic modulators of network activity. Front. Neural Circuits 12, 78.
Daubert, E.A., Condron, B.G., 2010. Serotonin: a regulator of neuronal morphology and circuitry. Trends Neurosci. 33 (9), 424–434.
Deodhar, D., Kupfermann, I., 2000. Studies of neuromodulation of oscillatory systems in *Aplysia*, by means of genetic algorithms. Adapt. Behav. 8 (3–4), 267–296.
Diekman, C.O., Thomas, P.J., Wilson, C.G., 2017. Eupnea, tachypnea, and autoresuscitation in a closed-loop respiratory control model. J. Neurophysiol. 118 (4), 2194–2215.
Evans, C.G., Vilim, F.S., Harish, O., Kupfermann, I., Weiss, K.R., Cropper, E.C., 1999. Modulation of radula opener muscles in *Aplysia*. J. Neurophysiol. 82 (3), 1339–1351.
Hargreaves, M., Spriet, L.L., 2020. Skeletal muscle energy metabolism during exercise. Nat. Metab. 2 (9), 817–828.
Hill, A.V., 1938. The heat of shortening and the dynamic constants of muscle. Proc. R. Soc. Lond. Ser. B- Biological Sci. 126 (843), 136–195.
Hooper, S.L., Brezina, V., Cropper, E.C., Weiss, K.R., 1999. Flexibility of muscle control by modulation of muscle properties. In: Beyond Neurotransmission: Neuromodulation and Its Importance for Information Processing. Oxford University Press, pp. 241–274.
Hultman, E., Greenhaff, P., 1991. Skeletal muscle energy metabolism and fatigue during intense exercise in man. Sci. Prog. (1933-) 361–370.
Hurwitz, I., Cropper, E., Vilim, F., Alexeeva, V., Susswein, A., Kupfermann, I., Weiss, K., 2000. Serotonergic and peptidergic modulation of the buccal mass protractor muscle (I2) in *Aplysia*. J. Neurophysiol. 84 (6), 2810–2820.
James, R.S., Navas, C.A., Herrel, A., 2007. How important are skeletal muscle mechanics in setting limits on jumping performance? J. Exp. Biol. 210 (6), 923–933.
Kandel, E.R., 1979. Behavioral Biology of *Aplysia*. a Contribution to the Comparative Study of Opisthobranch Molluscs. W.H. Freeman, San Francisco.
Kuo, A.D., 2002. The relative roles of feedforward and feedback in the control of rhythmic movements. Mot. Control. 6 (2), 129–145.
Kupfermann, I., 1974. Feeding behavior in *Aplysia*: a simple system for the study of motivation. Behav. Biol. 10 (1), 1–26.
Kupfermann, I., 1979. Modulatory actions of neurotransmitters. Annu. Rev. Neurosci. 2 (1), 447–465.
Lichtwark, G., Wilson, A., 2005. A modified Hill muscle model that predicts muscle power output and efficiency during sinusoidal length changes. J. Exp. Biol. 208 (15), 2831–2843.
Liessem, S., Kowatschew, D., Dippel, S., Blanke, A., Korsching, S., Guschlbauer, C., Hooper, S.L., Predel, R., Büschges, A., 2021. Neuromodulation can be simple: myoinhibitory peptide, contained in dedicated regulatory pathways, is the only neurally-mediated peptide modulator of stick insect leg muscle. J. Neurosci. 41 (13), 2911–2929.
Lu, H., McManus, J.M., Cullins, M.J., Chiel, H.J., 2015. Preparing the periphery for a subsequent behavior: motor neuronal activity during biting generates little force but prepares a retractor muscle to generate larger forces during swallowing in *Aplysia*. J. Neurosci. 35 (12), 5051–5066.
Lyttle, D.N., Gill, J.P., Shaw, K.M., Thomas, P.J., Chiel, H.J., 2017. Robustness, flexibility, and sensitivity in a multifunctional motor control model. Biol. Cybernet. 111, 25–47.
Magni, P., Dozio, E., Ruscica, M., Celotti, F., Masini, M.A., Prato, P., Broccoli, M., Mambro, A., More, M., Strollo, F., 2009. Feeding behavior in mammals including humans. Ann. New York Acad. Sci. 1163 (1), 221–232.
Mansour, T.E., 1959. Studies on the carbohydrate metabolism of the liver fluke *Fasciola hepatica*. Biochim. et Biophys. Acta 34, 456–464.
McManus, J.M., Lu, H., Chiel, H.J., 2012. An in vitro preparation for eliciting and recording feeding motor programs with physiological movements in *Aplysia californica*. J. Vis. Experiments: JoVE (70), 4320.
Miller, H.A., Huang, S., Dean, E.S., Schaller, M.L., Tuckowski, A.M., Munneke, A.S., Beydoun, S., Pletcher, S.D., Leiser, S.F., 2022. Serotonin and dopamine modulate aging in response to food odor and availability. Nat. Commun. 13 (1), 3271.
Misia, G., Evangelisti, C., Merino, J.P., Pitzalis, E., Abelairas, A.M., Mosquera, J., Criado, A., Prato, M., Silvestri, A., 2024. Design and optimization of an electrochemical sensor based on carbon nanotubes for the reliable voltammetric detection of serotonin in complex biological fluids. Carbon 229, 119550.
Moore, K., Milton, A., Gosselin, R., 1961. Effect of 5-hydroxytryptamine on the respiration of excised lamellibranch gill. Br. J. Pharmacol. Chemother. 17 (2), 278–285.
O'Mahony, S.M., Clarke, G., Borre, Y., Dinan, T.G., Cryan, J., 2015. Serotonin, tryptophan metabolism and the brain-gut-microbiome axis. Behav. Brain Res. 277, 32–48.
Oranth, A., Schultheis, C., Tolstenkov, O., Erbguth, K., Nagpal, J., Hain, D., Brauner, M., Wabnig, S., Costa, W.S., McWhirter, R.D., et al., 2018. Food sensation modulates locomotion by dopamine and neuropeptide signaling in a distributed neuronal network. Neuron 100 (6), 1414–1428.
Rangaraju, V., Calloway, N., Ryan, T.A., 2014. Activity-driven local ATP synthesis is required for synaptic function. Cell 156 (4), 825–835.
Rodríguez, F.A., Mader, A., 2011. Energy systems in swimming. In: World Book of Swimming: From Science To Performance. Nova Science Publishers Inc. New York, p. 225.
Shaw, K.M., Lyttle, D.N., Gill, J.P., Cullins, M.J., McManus, J.M., Lu, H., Thomas, P.J., Chiel, H.J., 2015. The significance of dynamical architecture for adaptive responses to mechanical loads during rhythmic behavior. J. Comput. Neurosci. 38, 25–51.
Spardy, L.E., Markin, S.N., Shevtsova, N.A., Prilutsky, B.I., Rybak, I.A., Rubin, J.E., 2011. A dynamical systems analysis of afferent control in a neuromechanical model of locomotion: I. Rhythm generation. J. Neural Eng. 8 (6), 065003.
Susswein, A., Gev, S., Feldman, E., Markovich, S., 1983. Activity patterns and time budgeting of *Aplysia fasciata* under field and laboratory conditions. Behav. Neural. Biol. 39 (2), 203–220.
Sutton, G., Szczecinski, N., Quinn, R., Chiel, H., 2023. Phase shift between joint rotation and actuation reflects dominant forces and predicts muscle activation patterns. PNAS Nexus 2 (10), pgad298.
Tesch, P.A., Colliander, E.B., Kaiser, P., 1986. Muscle metabolism during intense, heavy-resistance exercise. Eur. J. Appl. Physiol. 55, 362–366.
Twarog, B.M., 1968. Possible mechanism of action of serotonin on molluscan muscle. In: Advances in Pharmacology. vol. 6, Elsevier, pp. 5–15.
Wang, Y., Gill, J.P., Chiel, H.J., Thomas, P.J., 2021. Shape versus timing: linear responses of a limit cycle with hard boundaries under instantaneous and static perturbation. SIAM J. Appl. Dyn. Syst. 20 (2), 701–744.
Wang, Y., Gill, J.P., Chiel, H.J., Thomas, P.J., 2022. Variational and phase response analysis for limit cycles with hard boundaries, with applications to neuromechanical control problems. Biol. Cybernet. 116 (5–6), 687–710.
Webster-Wood, V.A., Gill, J.P., Thomas, P.J., Chiel, H.J., 2020. Control for multifunctionality: bioinspired control based on feeding in *Aplysia californica*. Biol. Cybernet. 114 (6), 557–588.
Weiss, K., Březina, V., Cropper, E., Hooper, S., Miller, M., Probst, W., Vilim, F., Kupfermann, I., 1992. Peptidergic co-transmission in *Aplysia*: functional implications for rhythmic behaviors. Experientia 48, 456–463.
Weiss, K.R., Cohen, J.L., Kupfermann, I., 1978. Modulatory control of buccal musculature by a serotonergic neuron (metacerebral cell) in *Aplysia*. J. Neurophysiol. 41 (1), 181–203.
Weiss, K., Kupfermann, I., 1976. Homology of the giant serotonergic neurons (metacerebral cells) in *Aplysia* and pulmonate molluscs. Brain Res. 117 (1), 33–49.
Yabut, J.M., Crane, J.D., Green, A.E., Keating, D.J., Khan, W.I., Steinberg, G.R., 2019. Emerging roles for serotonin in regulating metabolism: new implications for an ancient molecule. Endocr. Rev. 40 (4), 1092–1107.
Yu, S.-N., Crago, P.E., Chiel, H.J., 1999. Biomechanical properties and a kinetic simulation model of the smooth muscle I2 in the buccal mass of *Aplysia*. Biol. Cybernet. 81, 505–513.
Yu, Z., Rubin, J.E., Thomas, P.J., 2023. Sensitivity to control signals in triphasic rhythmic neural systems: a comparative mechanistic analysis via infinitesimal local timing response curves. Neural Comput. 35 (6), 1028–1085.
Yu, Z., Thomas, P.J., 2021. Dynamical consequences of sensory feedback in a half-center oscillator coupled to a simple motor system. Biol. Cybernet. 115 (2), 135–160.
Yu, Z., Thomas, P.J., 2022. A homeostasis criterion for limit cycle systems based on infinitesimal shape response curves. J. Math. Biol. 84 (4), 24.
Yu, Z., Thomas, P.J., 2024. Variational analysis of sensory feedback mechanisms in powerstroke–recovery systems. Biol. Cybernet. 118 (5), 277–309.
Zhurov, Y., Brezina, V., 2005. Temperature compensation of neuromuscular modulation in *Aplysia*. J. Neurophysiol. 94 (5), 3259–3277.